Targeting REGNASE-1 programs long-lived effector T cells for cancer therapy

https://doi.org/10.1038/s41586-019-1821-z

Received: 5 February 2019

Accepted: 7 November 2019

Published online: 11 December 2019

Jun Wei[1,5], Lingyun Long[1,5], Wenting Zheng[2], Yogesh Dhungana[1], Seon Ah Lim[1], Cliff Guy[1], Yanyan Wang[1], Yong-Dong Wang[3], Chenxi Qian[1,3], Beisi Xu[3], Anil KC[1], Jordy Saravia[1], Hongling Huang[1], Jiyang Yu[3], John G. Doench[4], Terrence L. Geiger[2] & Hongbo Chi[1]*

Adoptive cell therapy represents a new paradigm in cancer immunotherapy, but it can be limited by the poor persistence and function of transferred T cells[1]. Here we use an in vivo pooled CRISPR–Cas9 mutagenesis screening approach to demonstrate that, by targeting REGNASE-1, $CD8^+$ T cells are reprogrammed to long-lived effector cells with extensive accumulation, better persistence and robust effector function in tumours. REGNASE-1-deficient $CD8^+$ T cells show markedly improved therapeutic efficacy against mouse models of melanoma and leukaemia. By using a secondary genome-scale CRISPR–Cas9 screening, we identify BATF as the key target of REGNASE-1 and as a rheostat that shapes antitumour responses. Loss of BATF suppresses the increased accumulation and mitochondrial fitness of REGNASE-1-deficient $CD8^+$ T cells. By contrast, the targeting of additional signalling factors—including PTPN2 and SOCS1—improves the therapeutic efficacy of REGNASE-1-deficient $CD8^+$ T cells. Our findings suggest that T cell persistence and effector function can be coordinated in tumour immunity and point to avenues for improving the efficacy of adoptive cell therapy for cancer.

Adoptive cell therapy (ACT), including the use of T cells engineered to express chimeric antigen receptors (CARs), has produced unprecedented clinical outcomes for cancer immunotherapy. However, the therapeutic efficacy of ACT—especially in solid tumours—is often limited by the poor in vivo accumulation, persistence and function of adoptively transferred T cells[1]. Paradoxically, terminal effector $CD8^+$ T cells have been shown to have reduced antitumour efficacy and exhibit poor in vivo persistence[2]. How T cell fate decisions are regulated in the tumour microenvironment (TME) remains poorly understood.

Here, through an in vivo pooled CRISPR–Cas9 mutagenesis screening of metabolism-associated factors, we identify REGNASE-1 as a major negative regulator of antitumour responses. REGNASE-1-deficient $CD8^+$ T cells are reprogrammed in the TME to long-lived effector cells by enhancing BATF function and mitochondrial metabolism, thereby improving ACT for cancer.

Screen for metabolic regulators of ACT

T cell longevity and function in cancer immunotherapy have previously been proposed to closely correlate with cell metabolic fitness[3], although the underlying molecular mechanisms are unclear. To systematically investigate the roles of metabolism-associated factors in T-cell-mediated antitumour immunity, we developed a pooled CRISPR–Cas9 mutagenesis screening approach in an ACT model (Fig. 1a), using $CD8^+$ T cells that express the OT-I T cell receptor (TCR) and Cas9 as well as mice inoculated with B16 melanoma cells that express the cognate antigen (B16 Ova). We developed two lentiviral sub-libraries of single-guide (sg) RNAs (six sgRNAs per gene) targeting 3,017 metabolic enzymes, small molecule transporters and metabolism-related transcriptional regulators (Supplementary Table 1). Seven days after adoptive transfer, sgRNA-transduced OT-I cells in tumour-infiltrating lymphocytes were examined for library representation. A total of 218 genes were significantly depleted (Fig. 1b, Supplementary Table 2), including *Txnrd1*[4], *Ldha*[5], *Fth1*[6] and *Foxo1*[7], which are known regulators of cell survival and expansion. Notably, *Zc3h12a* (also known as *Regnase-1*, which encodes REGNASE-1) was the most highly enriched gene (Fig. 1b), which suggests that REGNASE-1 could be a major negative regulator of antitumour responses. REGNASE-1 is known to have RNase activity and to regulate activation of immune cells[8,9], but the function of REGNASE-1 in tumour immunity is currently unclear.

To validate our findings, we developed an in vivo dual transfer system to compare OT-I cells that were transduced with sgRNA vectors that express distinct fluorescent proteins in the same tumour-bearing host (Extended Data Fig. 1a, b), without there being noticeable effects of different fluorescent proteins per se (top panels in Extended Data Fig. 1c, d). We tested OT-I cells transduced with two different sgRNAs that target *Regnase-1*, and found that the relative proportion of REGNASE-1-null OT-I cells was markedly increased in both the spleen and tumour (Extended Data Fig. 1c–e). Imaging analysis identified significantly more REGNASE-1-null OT-I cells than wild-type control cells within tumours (Fig. 1c). Analysis of the targeting efficacy of guides revealed efficient disruption of *Regnase-1* (Extended Data Fig. 1f). Next, we examined the persistence of REGNASE-1-null OT-I cells at days 7, 14 and 21 after transfer. Whereas wild-type OT-I cells declined over time,

[1]Department of Immunology, St Jude Children's Research Hospital, Memphis, TN, USA. [2]Department of Pathology, St Jude Children's Research Hospital, Memphis, TN, USA. [3]Department of Computational Biology, St Jude Children's Research Hospital, Memphis, TN, USA. [4]Broad Institute of Harvard and MIT, Cambridge, MA, USA. [5]These authors contributed equally: Jun Wei, Lingyun Long. *e-mail: hongbo.chi@stjude.org

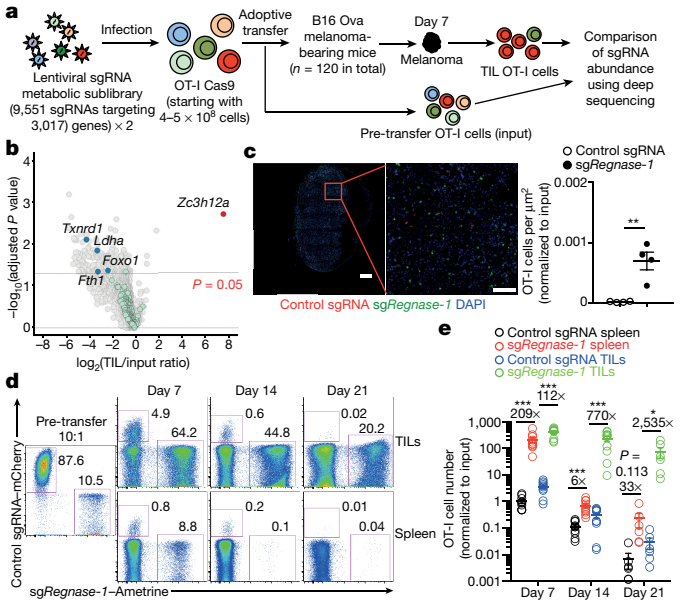

Fig. 1 | In vivo CRISPR–Cas9 screening identifies REGNASE-1 as a major negative regulator of the antitumour responses of CD8⁺ T cells. a, Diagram of CRISPR screening for metabolic regulators of ACT. TIL, tumour-infiltrating lymphocyte. **b**, Scatter plot of the enrichment of candidates ($n = 6$ sgRNAs per gene) with the most extensively enriched (red) and selectively depleted (blue) genes, as well as dummy genes (green; generated by random combinations of 6 out of 1,000 non-targeting control sgRNAs per dummy gene) highlighted. **c**, Representative images (left) and quantification of the relative OT-I cell number per area (μm²) normalized to input (right) in the tumour section ($n = 4$). OT-I cells transduced with control sgRNA (red) and sgRNA against *Regnase-1* (sg*Regnase-1*, green) were mixed at a 10:1 ratio and transferred into tumour-bearing mice, and analysed at day 7. Scale bars, 500 μm. **d**, **e**, OT-I cells transduced with control sgRNA or sgRNA against *Regnase-1* were mixed at a 10:1 ratio and transferred into tumour-bearing mice, followed by analysis of the proportion of OT-I cells in total CD8α⁺ cells (**d**) and quantification of normalized OT-I cell number relative to input (**e**) at day 7 ($n = 10$), day 14 ($n = 10$) and day 21 ($n = 6$). Cell numbers in the tumour are indicated per gram of tissue. Mean ± s.e.m. (**c**, **e**). $^*P < 0.05$, $^{**}P < 0.01$, $^{***}P < 0.001$. Two-tailed paired Student's *t*-test followed by Bonferroni correction (**b**) or two-tailed unpaired Student's *t*-test (**c**, **e**). Data are representative of two (**c**, **d**), or pooled from two (**e**), independent experiments.

REGNASE-1-null cells had markedly better persistence—especially in the tumour and at later time points (Fig. 1d, e). Therefore, the loss of REGNASE-1 endows tumour-specific CD8⁺ T cells with greatly improved accumulation and persistence, preferentially in the tumour.

Loss of REGNASE-1 improves ACT efficacy

We assessed the efficacy of REGNASE-1-null CD8⁺ T cells in ACT that targets a range of different tumours. In the B16 Ova model of melanoma, REGNASE-1-null OT-I cells showed much stronger antitumour effects than did wild-type cells, as evidenced by markedly inhibited tumour growth and the increased survival of melanoma-bearing mice (Fig. 2a, b). Similar results were observed in T cells that express the pme-1 TCR (which recognize the endogenous melanoma antigen gp100) when transferred into mice bearing B16 F10 melanoma (Fig. 2c, d). To assess the efficacy of CAR T cells against leukaemia, we used T cells that express CARs targeting human CD19 in combination with BCR–ABL1⁺ progenitor acute lymphoblastic leukaemia (Philadelphia-chromosome (Ph)⁺ B-ALL) cells[10] that express human CD19 (human CD19–Ph⁺ B-ALL cells). REGNASE-1-null CAR T cells showed a therapeutic efficacy that was much stronger than that of wild-type cells, as indicated by mouse survival (Fig. 2e) and tumour burden analyses

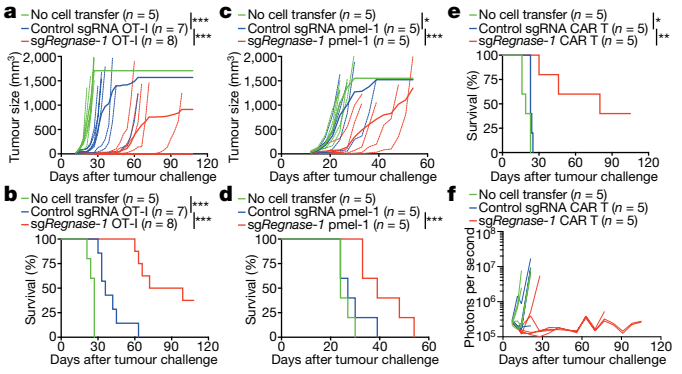

Fig. 2 | Deletion of REGNASE-1 enhances the efficacy of ACT against solid and blood cancers. a–**f**, OT-I (**a**, **b**), pmel-1 (**c**, **d**) or CD8⁺ CAR T (**e**, **f**) cells (5×10^6) transduced with non-targeting control sgRNA or sgRNA against *Regnase-1* were transferred into mice at day 12 after engraftment of B16 Ova (**a**, **b**) or B16 F10 (**c**, **d**) melanoma, or at day 7 after Ph⁺ B-ALL cell engraftment (**e**, **f**), followed by analyses of tumour size (**a**, **c**), mouse survival (**b**, **d**, **e**) and tumour burden via xenogen imaging of bioluminescent signal intensities (**f**). Non-treatment control mice received no transfer of T cells. $^*P < 0.05$, $^{**}P < 0.01$, $^{***}P < 0.001$. Two-way analysis of variance (ANOVA) (**a**, **c**) or log-rank (Mantel–Cox) test (**b**, **d**, **e**). Data are representative of two (**a**, **b**, **e**, **f**) or four (**c**, **d**) independent experiments.

(Fig. 2f). Collectively, REGNASE-1 deletion markedly enhances the efficacy of ACT against both solid and blood cancers.

REGNASE-1 loss reprograms T cells in TME

To address cell-intrinsic effects mediated by REGNASE-1, we performed RNA sequencing (RNA-seq) of REGNASE-1-null and wild-type OT-I cells isolated from the in vivo dual transfer system. Gene set enrichment analysis (GSEA) using gene modules associated with different functional states of tumour-infiltrating CD8⁺ T cells[11] revealed that tumour-infiltrating REGNASE-1-null cells were enriched with the naive or memory module (Fig. 3a). Gene targets that were repressed by REGNASE-1 were also enriched in memory-like CD8⁺ T cells in chronic infection[12,13] (Extended Data Fig. 2a, b). Accordingly, tumour-infiltrating REGNASE-1-null cells had increased expression of TCF-1 (a transcription factor that is associated with naive or memory T cells[14]) (Fig. 3b, Extended Data Fig. 2c) and *Lef1*, *Bach2*, *Tcf7* (which encodes TCF-1), *Foxp1*, *Bcl6* and *Fosb*[14–17], but had lower expression of *Irf2*, *Irf4* and *Hmgb2*[18,19] (Extended Data Fig. 2d–f). We next performed assay for transposase-accessible chromatin using sequencing (ATAC-seq)[20] to measure the chromatin accessibility of tumour-infiltrating REGNASE-1-null and wild-type cells. Motif searches on accessible regions identified an enrichment of TCF-1, BACH2 and BCL6—but downregulated IRF4 motifs—in REGNASE-1-null cells (Extended Data Fig. 2g, h). Thus, REGNASE-1-null CD8⁺ T cells are reprogrammed in the TME with enhanced gene-expression programs associated with naive or memory cells.

Transcriptional profiling revealed marked differences between tumour-infiltrating and peripheral REGNASE-1-null cells (Extended Data Fig. 2i). Unlike the enrichment of the naive or memory module in REGNASE-1-null cells in tumours (Fig. 3a), but consistent with previous reports that describe the negative role of REGNASE-1 in T cell activation under homeostasis[8,9], peripheral REGNASE-1-null cells were enriched with the activation-associated—but not with the naive or memory—module (Extended Data Fig. 2j), and had reduced expression of TCF-1 (Extended Data Fig. 2k). Given the TME-specific phenotypes of REGNASE-1-null cells, we assessed the regulation of REGNASE-1 and found lower expression of REGNASE-1 in tumour-infiltrating than in peripheral OT-I cells (Extended Data Fig. 3a). Additionally, gene targets repressed by REGNASE-1 were increased in tumour-infiltrating

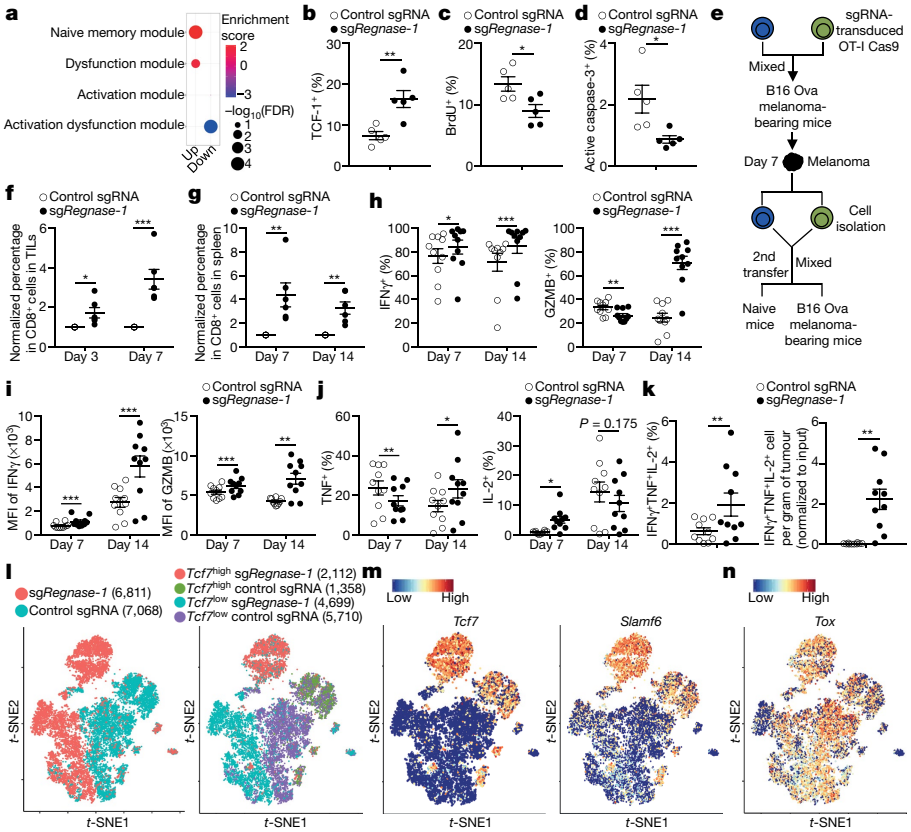

Fig. 3 | Deletion of REGNASE-1 reprograms tumour-infiltrating CD8⁺ T cells to long-lived effector cells. a, GSEA enrichment plots of RNA-seq analysis of OT-I cells, transduced with sgRNA against *Regnase-1* ($n = 5$) versus non-targeting control sgRNA, and isolated from tumour-infiltrating lymphocytes from the dual transfer system, using gene sets of the activation states of tumour-infiltrating CD8⁺ T cells[11]. **b**–**d**, Tumour-infiltrating OT-I cells transduced with sgRNA, from the dual transfer system ($n = 5$), were analysed at day 7 (**b**) and day 14 (**c**, **d**) for the quantification of frequencies of TCF-1⁺ (**b**), BrdU⁺ (**c**) and active caspase-3⁺ (**d**) cells. **e**–**g**, Diagram of in vivo persistence assay (**e**): sgRNA-transduced OT-I cells were isolated from tumour-infiltrating lymphocytes, mixed at a 1:1 ratio (1×10^5 each) and transferred into tumour-bearing hosts (**f**) or naive mice (**g**). Quantification of the normalized OT-I cell frequency in tumour-infiltrating lymphocytes of tumour-bearing hosts ($n = 6$) (**f**) or in the spleen of naive hosts ($n = 6$) (**g**). **h**–**k**, Tumour-infiltrating OT-I cells transduced with sgRNA, from the dual transfer system, were analysed at day 7 ($n = 10$) and day 14 ($n = 10$) for the quantification of frequencies of IFNγ⁺ cells (**h**, left), GZMB⁺ cells (**h**, right), TNF⁺ cells (**j**, left), IL-2⁺ cells (**j**, right) and polyfunctional IFNγ⁺TNF⁺IL-2⁺ cells (**k**, left) in OT-I cells, and mean fluorescence intensity (MFI) of IFNγ and GZMB in IFNγ⁺ and GZMB⁺ cells, respectively (**i**), and cell number (normalized to input) per gram of tumour (**k**, right) of polyfunctional IFNγ⁺TNF⁺IL-2⁺ OT-I cells. **l**–**n**, scRNA-seq analysis of tumour-infiltrating OT-I cells transduced with sgRNA, isolated from the dual transfer system at day 7. *t*-Distributed stochastic neighbour embedding (*t*-SNE) visualization of OT-I cells indicating genotypes (**l**, left), *Tcf7*^{high} and *Tcf7*^{low} cells (**l**, right), and *Tcf7* (**m**, left), *Slamf6* (**m**, right) and *Tox* (**n**) gene expression in individual cells. Mean ± s.e.m. (**b**–**d**, **f**–**k**). $^*P < 0.05$, $^{**}P < 0.01$, $^{***}P < 0.001$. Kolmogorov–Smirnov test followed by Benjamini–Hochberg correction (**a**), two-tailed unpaired Student's *t*-test (**b**–**d**, **f**, **g**) or two-tailed paired Student's *t*-test in (**h**–**k**). Data are representative of three (**b**), or pooled from two (**c**, **d**, **f**–**k**), independent experiments.

cells (Extended Data Fig. 3b), indicative of dampened REGNASE-1 activity. Moreover, stimulation with TCR—and, to a lesser extent, IL-2 or IL-21—induced REGNASE-1 cleavage[9] (Extended Data Fig. 3c). Antigen recognition was crucial in driving the CD8⁺ T cell accumulation in tumour-infiltrating lymphocytes upon deletion of REGNASE-1, as indicated by reduced REGNASE-1-null OT-I cells in mice that bear B16 F10 melanoma (without the cognate antigen) compared to B16 Ova melanoma (Extended Data Fig. 3d). Antigen stimulation was also required for REGNASE-1-null cells to acquire increased TCF-1 expression (Extended Data Fig. 3e). By contrast, hypoxia did not alter the expression of REGNASE-1 or immune markers (Extended Data Fig. 3f, g). Thus, REGNASE-1-null CD8⁺ T cells undergo specific reprogramming in the TME in a process downstream of tumour antigen stimulation.

We next determined the cellular homeostasis of REGNASE-1-null cells. GSEA revealed that cell-cycling-associated hallmarks were the top downregulated pathways in tumour-infiltrating REGNASE-1-null cells (Extended Data Fig. 4a, b). Accordingly, these cells had reduced BrdU and Ki-67 staining at day 14 after adoptive transfer (Fig. 3c, Extended Data Fig. 4c), albeit not at day 7 (Extended Data Fig. 4d, e). Also, tumour-infiltrating REGNASE-1-null cells had reduced levels of active caspase-3 (Fig. 3d, Extended Data Fig. 4f) and DNA damage biomarker (Extended Data Fig. 4g). Therefore, tumour-infiltrating REGNASE-1-null cells are less proliferative after effector expansion and show better survival than wild-type cells. By contrast (but consistent with the increased activation signatures; Extended Data Fig. 2j), peripheral REGNASE-1-null cells were enriched with signatures associated with cell cycling and apoptosis (Extended Data Fig. 4h), which was validated by increased BrdU and active caspase-3 staining (Extended Data Fig. 4i, j). These results further support the TME-specific phenotypes of REGNASE-1-null CD8⁺ T cells. To test the effect on in vivo persistence, we isolated wild-type and REGNASE-1-null OT-I cells from tumour-infiltrating lymphocytes and cotransferred them into tumour-bearing or naive hosts (Fig. 3e). REGNASE-1-null cells showed increased accumulation in tumour sites (Fig. 3f) as well as in the spleen of naive recipients (Fig. 3g). These analyses collectively indicate that tumour-infiltrating REGNASE-1-null CD8⁺ T cells are characterized by in vivo quiescence and survival, with better persistence than wild-type CD8⁺ T cells in response to both antigenic and homeostatic signals.

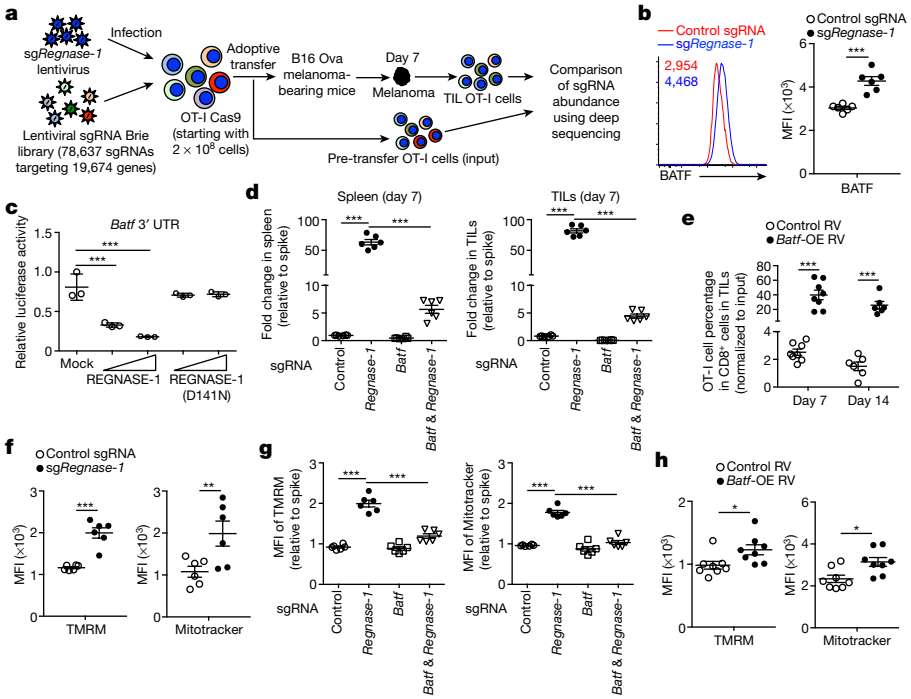

Fig. 4 | BATF is a key REGNASE-1 functional target for mediating mitochondrial fitness and effector responses. a, Diagram of secondary genome-scale CRISPR screening. **b**, Tumour-infiltrating OT-I cells transduced with sgRNA, from the dual transfer system ($n = 6$), were analysed at day 7 for BATF expression (left) and quantification of BATF MFI (right). **c**, Luciferase activity of HEK293T cells after transfection with *Batf* mRNA 3′ UTR reporter, together with control (mock), wild-type or REGNASE-1(D141N)-expressing plasmid ($n = 3$). **d**, **e**, In vivo accumulation of OT-I cells transduced with an individual sgRNA or with two sgRNAs (**d**) or *Batf*-overexpressing (OE) retrovirus (RV) (**e**) in the dual transfer system ($n = 6$). The OT-I cell percentage in CD8α$^+$ cells was normalized to co-transferred spike cells transduced with the non-targeting control sgRNA (**d**). **f**–**h**, Tumour-infiltrating OT-I cells transduced with an individual sgRNA (**f**; $n = 6$), individual or two sgRNAs (**g**; $n = 6$) or *Batf*-overexpressing retrovirus (**h**; $n = 8$) from the dual transfer system were analysed at day 7 for the quantification of the MFI of tetramethylrhodamine, methyl ester (TMRM) (left) and Mitotracker (right). The MFIs of TMRM and Mitotracker were normalized to those of co-transferred spike cells transduced with control sgRNA (**g**). Mean ± s.e.m. (**b**, **d**–**h**) or mean ± s.d. (**c**). $^*P < 0.05$, $^{**}P < 0.01$, $^{***}P < 0.001$. Two-tailed unpaired Student's *t*-test (**b**, **e**, **h**), one-way ANOVA (**c**, **d**, **g**) or two-tailed paired Student's *t*-test (**f**). Data are representative of two (**c**), or pooled from two (**b**, **d**–**h**), independent experiments.

Although in tumours REGNASE-1-null OT-I cells acquired programs associated with naive or memory cells, these cells had higher expression of many activation-associated markers (Extended Data Fig. 5a), retained an effector surface phenotype (CD44$^+$CD62L$^-$) (Extended Data Fig. 5b), and expressed more IFNγ and granzyme B (GZMB) (Fig. 3h, i, Extended Data Fig. 5c, d). Additionally, these cells had similar or enhanced capacities to produce TNF and IL-2 (Fig. 3j, Extended Data Fig. 5e, f), and contained an increased number of IFNγ$^+$TNF$^+$IL-2$^+$ polyfunctional cells (Fig. 3k). Thus, although tumour-infiltrating CD8$^+$ T cells that lack REGNASE-1 acquire better persistence and a survival advantage, they retain potent effector function.

We used single-cell (sc)RNA-seq[21] to investigate the heterogeneity of tumour-infiltrating lymphocytes isolated from the in vivo dual transfer system. REGNASE-1-null OT-I cells had patterns that were distinct from those of wild-type cells, including an increased proportion of *Tcf7*^{high} cells (Fig. 3l, m). In both genotypes, *Tcf7*^{high} cells expressed *Tox*[22,23] (Fig. 3n) and—compared with *Tcf7*^{low} cells—had reduced expression of *Pdcd1* (which encodes PD-1) and *Havcr2* (which encodes TIM3) (Extended Data Fig. 6a). Wild-type *Tcf7*^{high} cells were enriched with the TCF-1 target gene *Slamf6*[23,24] and memory-like gene signatures[12,13], which were further increased in REGNASE-1-null cells (Fig. 3m, Extended Data Fig. 6b). By contrast, wild-type *Tcf7*^{high} cells had a lower expression of *Ifng* and *Gzmb* than did *Tcf7*^{low} cells, but in the absence of REGNASE-1, *Ifng* and *Gzmb* were increased in both *Tcf7*^{high} and *Tcf7*^{low} cells (Extended Data Fig. 6c). Moreover, in REGNASE-1-null OT-I cells, the effector cell factor *Batf*[25,26]—but not *Id2*[27]—was highly expressed by both *Tcf7*^{high} and *Tcf7*^{low} cells (Extended Data Fig. 6d, e). Flow cytometry validation revealed that TCF-1$^+$ cells expressed TOX and SLAMF6 (with modestly higher levels observed in REGNASE-1-null cells), but had low levels of expression of KLRG1 and TIM3 and intermediate levels of expression of PD-1 (Extended Data Fig. 6f). Collectively, these results establish the dual roles of REGNASE-1 in coordinating T cell effector function and memory-like features in antitumour immunity.

REGNASE-1–BATF shapes effector responses

To identify the mechanisms that underlie REGNASE-1 signalling, we took advantage of the extensive accumulation of tumour-infiltrating REGNASE-1-null cells and performed a secondary in vivo genome-scale CRISPR screening by cotransducing OT-I cells with sgRNA targeting *Regnase-1* and the Brie lentiviral genome-scale sgRNA library[28] (Fig. 4a). A total of 331 genes were strongly depleted in the screening, including *Slc7a5*[29], *Itk*[30], *Prkaa1*[31], *Mapk1*[32] and *Tbx21*[33] (Extended Data Fig. 7a, Supplementary Table 3). Given the role of REGNASE-1 in inhibiting gene expression[8,9], we applied two criteria to identify the functional targets of REGNASE-1: candidates should be upregulated in REGNASE-1-null cells in RNA-seq data, but depleted in tumour-infiltrating lymphocytes in the genome-scale CRISPR screening. This analysis revealed two candidates, one of which was *Batf*[25,26] (Extended Data Fig. 7b). REGNASE-1-null cells showed increased expression of BATF (Fig. 4b, Extended Data Fig. 6d) and enrichment of BATF-binding motifs and gene targets[26] (Extended Data Figs. 2g, 7c, d). We next determined whether *Batf* mRNA is regulated by REGNASE-1, using the 3′ untranslated region (UTR) of the *Il2* and *Il4* genes as positive and negative controls, respectively[9] (Extended Data Fig. 7e). The 3′ UTR of *Batf* gene was dose-dependently inhibited by REGNASE-1, but not by the nuclease-inactive mutant REGNASE-1(D141N)

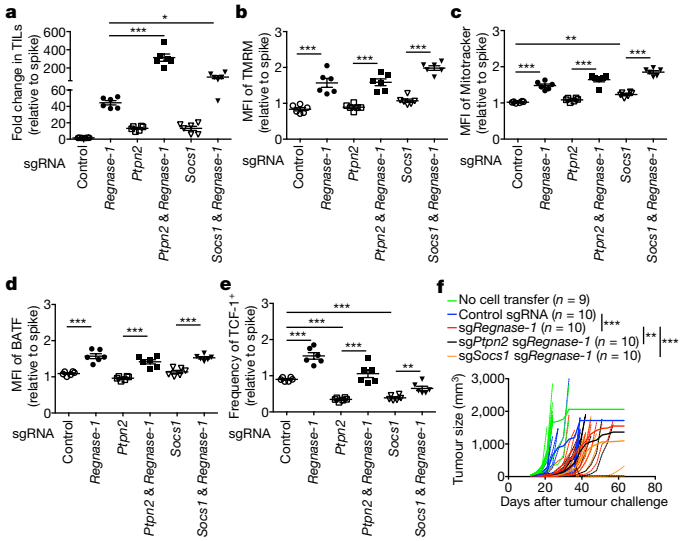

Fig. 5 | Genome-scale CRISPR screening identifies PTPN2 and SOCS1 as additional targets for enhancing the antitumour activity of REGNASE-1-null CD8$^+$ T cells. a–**e**, OT-I cells transduced with non-targeting control sgRNA (spike) were mixed at a 1:1 ratio with cells transduced with non-targeting control sgRNA, sgRNA against *Regnase-1*, sgRNA against *Ptpn2*, sgRNAs against *Ptpn2* and *Regnase-1*, sgRNA against *Socs1* or sgRNAs against *Socs1* and *Regnase-1*, and transferred into tumour-bearing hosts individually ($n = 6$). Tumour-infiltrating OT-I cells were analysed at day 7 for quantification of relative OT-I cell percentage in CD8α$^+$ cells normalized to spike (**a**), quantification of relative MFI of TMRM (**b**), Mitotracker (**c**) and BATF (**d**) normalized to spike, and quantification of the relative frequency of TCF-1$^+$ cells normalized to spike (**e**). **f**, Pmel-1 cells transduced with an individual control sgRNA, sgRNA against *Regnase-1* or with two sgRNAs (against *Regnase-1* and either *Ptpn2* (sg*Ptpn2*) or *Socs1* (sg*Socs1*)) (4×10^6 cells in each group) were transferred into mice at day 12 after engraftment of B16 F10 melanoma, followed by analysis of tumour size. Non-treatment control mice received no transfer of T cells. Mean ± s.e.m. (**a**–**e**). $^*P < 0.05$, $^{**}P < 0.01$, $^{***}P < 0.001$. One-way ANOVA (**a**–**e**) or two-way ANOVA (**f**). Data in **a**–**f** are pooled from two independent experiments.

(Fig. 4c), which reveals that BATF is a target of REGNASE-1. Importantly, co-deletion of BATF (Extended Data Fig. 7f, g) markedly reduced the accumulation of REGNASE-1-null OT-I cells in both the periphery and tumour (Fig. 4d, Extended Data Fig. 7h), associated with increased active caspase-3 (Extended Data Fig. 7i). By contrast, cells deficient in both BATF and REGNASE-1 still had increased TCF-1 expression compared to wild-type cells (Extended Data Fig. 7j), which suggests a dispensable role of BATF in TCF-1 expression. Moreover, BATF co-deletion blocked the increased IFNγ production in REGNASE-1-null cells, and dampened the antitumour effects of REGNASE-1-null cells in the pmel-1 ACT model (Extended Data Fig. 7k, l). Therefore, REGNASE-1 targets BATF to impair the accumulation and effector function, but not the TCF-1 expression, of tumour-specific T cells.

BATF expression was aberrantly induced in REGNASE-1-null cells in response to TCR and to, a lesser extent, IL-2—but not IL-21 (Extended Data Fig. 8a). To test whether BATF is a limiting factor in antitumour responses, we transduced wild-type OT-I cells with BATF (Extended Data Fig. 8b) and found that BATF overexpression improved cell accumulation in the spleen (Extended Data Fig. 8c, d) and even more markedly in the tumour (Fig. 4e, Extended Data Fig. 8c). Accordingly, BATF-overexpressing OT-I cells in the tumour had increased cell proliferation and modestly reduced active caspase-3 (Extended Data Fig. 8e, f), and produced more IFNγ, GZMB and TNF (but not IL-2) (Extended Data Fig. 8g). By contrast (but consistent with the role of BATF in promoting effector differentiation[26]), TCF-1 expression was reduced in cells that overexpress BATF (Extended Data Fig. 8h). Therefore, BATF is regulated by REGNASE-1 and immune signals and acts as an important rheostat in mediating antitumour effector responses.

To determine the contribution of aberrant BATF expression to the altered chromatin accessibility in REGNASE-1-null cells, we performed ATAC-seq analysis of wild-type, REGNASE-1-null cells, BATF-null cells, and cells deficient for both REGNASE-1 and BATF isolated from tumour-infiltrating lymphocytes. We identified 7,480 genes with increased chromatin accessibility in REGNASE-1-null cells as compared to wild-type cells (Extended Data Fig. 9a), and BATF co-deletion reversed the upregulation of a large proportion of these genes (5,052 genes in total) (Extended Data Fig. 9a). In addition, 2,527 of these 5,052 genes showed downregulated chromatin accessibility in BATF-null cells as compared to wild-type cells (Extended Data Fig. 9a). Thus, a large majority of the genes with increased chromatin accessibility in REGNASE-1-null cells are BATF-dependent.

We next determined the functional pathways by which REGNASE-1 regulates antitumour immunity. Functional enrichment of the top-ranking depleted genes of the genome-scale CRISPR screening revealed the oxidative phosphorylation (OXPHOS) hallmark as the top-enriched pathway (Extended Data Fig. 9b). OXPHOS was also the top-ranking gene set enriched in tumour-infiltrating REGNASE-1-null cells relative to wild-type cells (Extended Data Figs. 4a, 9c). Although mitochondrial metabolism correlates with T cell fitness and antitumour activity[34,35], the negative signals involved—especially in the TME—remain unknown. REGNASE-1-null cells showed increased mitochondrial fitness, as indicated by increased mitochondrial mass, membrane potential and volume (Fig. 4f, Extended Data Fig. 9d), as well as higher basal and maximal oxygen consumption rates (Extended Data Fig. 9e). Compared with REGNASE-1-null cells, cells deficient in both BATF and REGNASE-1 downregulated hallmarks associated with OXPHOS and cell cycling (Extended Data Fig. 9f, g). Moreover, BATF co-deletion largely blocked the increased mitochondrial mass and membrane potential in REGNASE-1-null cells at day 5 and day 7 after adoptive transfer (Fig. 4g, Extended Data Fig. 9h). Conversely, BATF overexpression was sufficient to upregulate mitochondrial mass and membrane potential (Fig. 4h). These results collectively reveal a role of BATF in linking REGNASE-1 function and mitochondrial fitness.

To understand the molecular basis for the REGNASE-1- and BATF-mediated regulation of mitochondrial fitness, we mined our ATAC-seq data for altered chromatin accessibility of mitochondrial genes. A total of 341 mitochondrial genes showed significantly upregulated chromatin accessibility in the absence of REGNASE-1, and 214 of these genes were blocked by BATF co-deletion (Extended Data Fig. 9i). Moreover, 96 of these 214 genes showed downregulated chromatin accessibility in BATF-null cells as compared to wild-type cells (Extended Data Fig. 9i). These results further support a crucial contribution of BATF to the enhanced mitochondrial function in the absence of REGNASE-1.

Combination therapy with PTPN2 and SOCS1

Combination therapy is key to the clinical success of cancer immunotherapies[36]. To identify whether the therapeutic potential of REGNASE-1-null CD8$^+$ T cells could be further potentiated, we focused on the top two genes that were enriched in tumour-infiltrating lymphocytes in our genome-scale CRISPR screening: *Ptpn2* and *Socs1*(Extended Data Fig. 7a). We validated the effects of co-deletion of these genes to enhance the accumulation of tumour-infiltrating REGNASE-1-null cells (Fig. 5a, Extended Data Fig. 10a). Deletion of PTPN2 or SOCS1 alone resulted in a modestly increased accumulation of OT-I cells in the tumour (Fig. 5a). Of note, SOCS1 has previously been identified to restrain human T cell proliferation in vitro[37], and PTPN2 deletion sensitizes cancer cells to immune checkpoint therapy[38]. Unlike BATF expression, the expression of PTPN2 or SOCS1 was not affected by

REGNASE-1 deletion (Extended Data Fig. 10b). Deletion of PTPN2 or SOCS1 alone either did not affect, or slightly increased, mitochondrial mass and membrane potential (Fig. 5b, c), and co-deletion of REGNASE-1 still increased these mitochondrial profiles (Fig. 5b, c). Furthermore, deletion of PTPN2 or SOCS1 did not affect BATF expression (Fig. 5d), but significantly reduced TCF-1 expression (Fig. 5e); REGNASE-1 co-deletion was still capable of upregulating TCF-1 expression (Fig. 5e). These comparative analyses reveal that the mechanisms exerted by PTPN2 or SOCS1 are largely discrete from those of REGNASE-1, including the effects on mitochondrial fitness and the regulation of BATF and TCF-1 expression.

We assessed the therapeutic efficacy of pmel-1 T cells with co-deletion of PTPN2 and REGNASE-1 or of SOCS1 and REGNASE-1. Although REGNASE-1 deletion alone greatly improved the therapeutic efficacy, pmel-1 T cells double-deficient for PTPN2 and REGNASE-1 or SOCS1 and REGNASE-1 exhibited additional effects at delaying tumour growth (Fig. 5f). Altogether, our CRISPR screening identifies targets that can be potentially combined with REGNASE-1 deletion in cancer immunotherapy.

Discussion

There is a great need to understand how cell-fate decisions occur in tumour-specific CD8$^+$ T cells. Here we reveal that tumour-specific CD8$^+$ T cells can be reprogrammed in the TME to acquire extensive accumulation and increased features associated with naive or memory cells for long-term persistence, while still retaining robust effector function (Extended Data Fig. 10c). REGNASE-1 is a major regulator that can be targeted to unleash this unique reprogramming in the TME, with marked therapeutic efficacy against both solid and blood cancers in ACT. The specific transcriptional adaptation of REGNASE-1-null CD8$^+$ T cells in the TME highlights a previously unappreciated function of REGNASE-1 after initial T cell activation[8,9], to enable the precise temporal and spatial control of T cell responses.

Despite the recent emphasis on the metabolic control of T cell activation and differentiation, the metabolic reprogramming and the molecular events involved remain to be explored in antitumour T cell responses[3]. Our results highlight the fact that REGNASE-1 restrains mitochondrial metabolism and effector responses through a key gene target, BATF. BATF acts as a limiting factor for programming antitumour responses and mitochondrial metabolism, thereby advancing our understanding of context-dependent roles of the pioneer factor BATF in adaptive immunity[26,39]. The genome-scale CRISPR screening also reveals PTPN2 and SOCS1 as potential targets to combine with REGNASE-1 deletion to boost antitumour immunity. From a therapeutic perspective, our findings have identified targets for ACT against both solid and blood cancers and point to avenues to reprogramming T cell state and metabolism in cancer immunity and immunotherapy.

Online content

Any methods, additional references, Nature Research reporting summaries, source data, extended data, supplementary information, acknowledgements, peer review information; details of author contributions and competing interests; and statements of data and code availability are available at https://doi.org/10.1038/s41586-019-1821-z.

1. Lim, W. A. & June, C. H. The principles of engineering immune cells to treat cancer. *Cell* **168**, 724–740 (2017).
2. Gattinoni, L. et al. Acquisition of full effector function *in vitro* paradoxically impairs the *in vivo* antitumor efficacy of adoptively transferred CD8$^+$ T cells. *J. Clin. Invest.* **115**, 1616–1626 (2005).
3. Kishton, R. J., Sukumar, M. & Restifo, N. P. Metabolic regulation of T cell longevity and function in tumor immunotherapy. *Cell Metab.* **26**, 94–109 (2017).
4. Muri, J. et al. The thioredoxin-1 system is essential for fueling DNA synthesis during T-cell metabolic reprogramming and proliferation. *Nat. Commun.* **9**, 1851 (2018).
5. Peng, M. et al. Aerobic glycolysis promotes T helper 1 cell differentiation through an epigenetic mechanism. *Science* **354**, 481–484 (2016).
6. Vanoaica, L. et al. Conditional deletion of ferritin H in mice reduces B and T lymphocyte populations. *PLoS ONE* **9**, e89270 (2014).
7. Ouyang, W., Beckett, O., Flavell, R. A. & Li, M. O. An essential role of the Forkhead-box transcription factor Foxo1 in control of T cell homeostasis and tolerance. *Immunity* **30**, 358–371 (2009).
8. Matsushita, K. et al. Zc3h12a is an RNase essential for controlling immune responses by regulating mRNA decay. *Nature* **458**, 1185–1190 (2009).
9. Uehata, T. et al. Malt1-induced cleavage of regnase-1 in CD4$^+$ helper T cells regulates immune activation. *Cell* **153**, 1036–1049 (2013).
10. Churchman, M. L. et al. Synergism of FAK and tyrosine kinase inhibition in Ph$^+$ B-ALL. *JCI Insight* **1**, 86082 (2016).
11. Singer, M. et al. A distinct gene module for dysfunction uncoupled from activation in tumor-infiltrating T cells. *Cell* **166**, 1500–1511 (2016).
12. Im, S. J. et al. Defining CD8$^+$ T cells that provide the proliferative burst after PD-1 therapy. *Nature* **537**, 417–421 (2016).
13. Leong, Y. A. et al. CXCR5$^+$ follicular cytotoxic T cells control viral infection in B cell follicles. *Nat. Immunol.* **17**, 1187–1196 (2016).
14. Zhou, X. et al. Differentiation and persistence of memory CD8$^+$ T cells depend on T cell factor 1. *Immunity* **33**, 229–240 (2010).
15. Hurton, L. V. et al. Tethered IL-15 augments antitumor activity and promotes a stem-cell memory subset in tumor-specific T cells. *Proc. Natl Acad. Sci. USA* **113**, E7788–E7797 (2016).
16. Roychoudhuri, R. et al. BACH2 regulates CD8$^+$ T cell differentiation by controlling access of AP-1 factors to enhancers. *Nat. Immunol.* **17**, 851–860 (2016).
17. Ichii, H., Sakamoto, A., Kuroda, Y. & Tokuhisa, T. Bcl6 acts as an amplifier for the generation and proliferative capacity of central memory CD8$^+$ T cells. *J. Immunol.* **173**, 883–891 (2004).
18. Man, K. et al. Transcription factor IRF4 promotes CD8+ T cell exhaustion and limits the development of memory-like T cells during chronic infection. *Immunity* **47**, 1129–1141 (2017).
19. Sade-Feldman, M. et al. Defining T cell states associated with response to checkpoint immunotherapy in melanoma. *Cell* **175**, 998–1013 (2018).
20. Buenrostro, J. D., Giresi, P. G., Zaba, L. C., Chang, H. Y. & Greenleaf, W. J. Transposition of native chromatin for fast and sensitive epigenomic profiling of open chromatin, DNA-binding proteins and nucleosome position. *Nat. Methods* **10**, 1213–1218 (2013).
21. Macosko, E. Z. et al. Highly parallel genome-wide expression profiling of individual cells using nanoliter droplets. *Cell* **161**, 1202–1214 (2015).
22. Khan, O. et al. TOX transcriptionally and epigenetically programs CD8$^+$ T cell exhaustion. *Nature* **571**, 211–218 (2019).
23. Miller, B. C. et al. Subsets of exhausted CD8$^+$ T cells differentially mediate tumor control and respond to checkpoint blockade. *Nat. Immunol.* **20**, 326–336 (2019).
24. Utzschneider, D. T. et al. T cell factor 1-expressing memory-like CD8$^+$ T cells sustain the immune response to chronic viral infections. *Immunity* **45**, 415–427 (2016).
25. Ciofani, M. et al. A validated regulatory network for Th17 cell specification. *Cell* **151**, 289–303 (2012).
26. Kurachi, M. et al. The transcription factor BATF operates as an essential differentiation checkpoint in early effector CD8$^+$ T cells. *Nat. Immunol.* **15**, 373–383 (2014).
27. Yang, C. Y. et al. The transcriptional regulators Id2 and Id3 control the formation of distinct memory CD8$^+$ T cell subsets. *Nat. Immunol.* **12**, 1221–1229 (2011).
28. Doench, J. G. et al. Optimized sgRNA design to maximize activity and minimize off-target effects of CRISPR–Cas9. *Nat. Biotechnol.* **34**, 184–191 (2016).
29. Sinclair, L. V. et al. Control of amino-acid transport by antigen receptors coordinates the metabolic reprogramming essential for T cell differentiation. *Nat. Immunol.* **14**, 500–508 (2013).
30. Atherly, L. O., Brehm, M. A., Welsh, R. M. & Berg, L. J. Tec kinases Itk and Rlk are required for CD8$^+$ T cell responses to virus infection independent of their role in CD4$^+$ T cell help. *J. Immunol.* **176**, 1571–1581 (2006).
31. Blagih, J. et al. The energy sensor AMPK regulates T cell metabolic adaptation and effector responses *in vivo*. *Immunity* **42**, 41–54 (2015).
32. D'Souza, W. N., Chang, C. F., Fischer, A. M., Li, M. & Hedrick, S. M. The Erk2 MAPK regulates CD8 T cell proliferation and survival. *J. Immunol.* **181**, 7617–7629 (2008).
33. Sullivan, B. M., Juedes, A., Szabo, S. J., von Herrath, M. & Glimcher, L. H. Antigen-driven effector CD8 T cell function regulated by T-bet. *Proc. Natl Acad. Sci. USA* **100**, 15818–15823 (2003).
34. Geiger, R. et al. l-Arginine modulates T cell metabolism and enhances survival and anti-tumor activity. *Cell* **167**, 829–842 (2016).
35. Kawalekar, O. U. et al. Distinct signaling of coreceptors regulates specific metabolism pathways and impacts memory development in CAR T cells. *Immunity* **44**, 380–390 (2016).
36. Sharma, P. & Allison, J. P. The future of immune checkpoint therapy. *Science* **348**, 56–61 (2015).
37. Shifrut, E. et al. Genome-wide CRISPR screens in primary human T cells reveal key regulators of immune function. *Cell* **175**, 1958–1971 (2018).
38. Manguso, R. T. et al. *In vivo* CRISPR screening identifies *Ptpn2* as a cancer immunotherapy target. *Nature* **547**, 413–418 (2017).
39. Quigley, M. et al. Transcriptional analysis of HIV-specific CD8$^+$ T cells shows that PD-1 inhibits T cell function by upregulating BATF. *Nat. Med.* **16**, 1147–1151 (2010).

Methods

No statistical methods were used to predetermine sample size. The experiments were not randomized and investigators were not blinded to allocation during experiments and outcome assessment.

Cell lines and mice

The B16 F10 cell line was purchased from ATCC. The B16 Ova cell line was provided by D. Vignali. The human CD19-Ph$^+$ B-ALL cell line was provided by T. Geiger (manuscript in preparation). C57BL/6, OT-I, pmel-1 and *Rosa26-Cas9* knock-in mice[40] were purchased from The Jackson Laboratory. CAR T transgenic mice (T cells express CARs that consist of anti-human CD19 (human CD19) scFv fragments, CD8 transmembrane domain and 4-1BB-CD3ζ signalling tail) were provided by T. Geiger (manuscript in preparation). We crossed *Rosa26-Cas9* knock-in mice[40] with OT-I[41], pmel-1[42] or CAR T transgenic mice to express Cas9 in antigen-specific CD8$^+$ T cells. Sex-matched mice were used at 7–16 weeks old unless otherwise noted. All mice were kept in a specific-pathogen-free facility in the Animal Resource Center at St Jude Children's Research Hospital. Experiments and procedures were performed in accordance with the Institutional Animal Care and Use Committee of St Jude Children's Research Hospital.

Cell purification and viral transduction

Naive Cas9-expressing OT-I cells were isolated from the spleen and peripheral lymph nodes (PLNs) of Cas9-OT-I mice using a naive CD8α$^+$ T cell isolation kit (Miltenyi Biotec 130-096-543) according to the manufacturer's instructions. Purified naive OT-I cells were activated in vitro for 18 h with 10 μg/ml anti-CD3 (2C11; Bio X Cell), 5 μg/ml anti-CD28 (37.51; Bio X Cell) before viral transduction. Viral transduction was performed by spin-infection at 800*g* at 25 °C for 3 h with 10 μg/ml polybrene (Sigma). Cells were cultured with human IL-2 (20 IU/ml; PeproTech), mouse IL-7 (2.5 ng/ml; PeproTech) and IL-15 (25 ng/ml; PeproTech) for 3–4 days. Transduced cells were sorted using a Reflection cell sorter (iCyt) before adoptive transfer into recipients. sgRNAs were designed by using the online tool (https://portals.broadinstitute.org/gpp/public/analysis-tools/sgrna-design). sgRNAs used in this study were as follows: non-targeting control sgRNA, ATGACACTTACGGTACTCGT; *Regnase-1* sgRNA, AAGGCAGTGGTTTCTTACGA; *Regnase-1* sgRNA no. 2, GGAGTGGAAACGCTTCATCG; *Batf* sgRNA, AGAGATCAAACAGCTCACCG; *Batf* sgRNA no. 2, AGGACTCATCTGATGATGTG (which gave results similar to those of *Batf* sgRNA; data not shown); *Ptpn2* sgRNA, AAGAAGTTACATCTTAACAC; *Ptpn2* sgRNA no. 2: CACTCTATGAGGATAGTCAT (which gave results similar to those of as *Ptpn2* sgRNA; data not shown); *Socs1* sgRNA, TGATGCGCCGGTAATCGGAG; *Socs1* sgRNA no. 2, TGGTGCGCGACAGTCGCCAA (which gave results similar to those of *Socs1* sgRNA; data not shown). The coding sequence of *Batf* (Addgene no. 34575) was subcloned into pMIG-II retroviral vector (Addgene no. 52107), which was co-transfected into Plat-E cells with the helper plasmid pCL-Eco (Addgene no. 12371) for the production of retrovirus.

Lentiviral sgRNA metabolic library CRISPR–Cas9 mutagenesis screening

Lentiviral and retroviral sgRNA vector design. The lentiviral sgRNA vector was generated from lentiGuide-puro vector by replacing the EF-1α PuroR fragment with a mouse PGK promoter-driven ametrine (or GFP or mCherry) fluorescent protein. The retroviral sgRNA vector was generated from pLMPd-Amt vector[43] by replacing the miR30 shRNA cassette with the U6-promoter-driven gRNA cassette from the lentiGuide-puro vector.

Lentiviral sgRNA metabolic library construction. The gene list (3,017 genes) of the mouse metabolic library was based on reported human metabolic genes[44]. A total of six gRNAs were designed for each mouse metabolic gene according to previously published selection criteria[45] and were split into two sub-libraries (AAAQ05 and AAAR07; Supplementary Table 1), each containing 500 non-targeting controls. Oligonucleotides containing the guide sequence were synthesized (Custom Array), PCR-amplified and cloned into the recipient vector via a Golden Gate cloning procedure, including 5 μl Tango Buffer (ThermoFisher), 5 μl dithiothreitol (10 mM stock), 5 μl ATP (10 mM stock), 500 ng vector (pre-digested with Esp3I, gel-extracted and isopropanol-precipitation-purified), 100 ng insert PCR product, 1 μl Esp3I (ThermoFisher ER0452), 1 μl T7 ligase (Enzymatics, 3,000 U/μl, L6020L) and water, up to 50 μl, and incubated in a cycle (5 min at 37 °C and 5 min at 20 °C) for 100 times. The product was then purified by isopropanol precipitation and electroporated into STBL4 cells (Life Technologies 11635018). The distribution of the library was determined by Illumina sequencing.

In vivo screening. Lentivirus was produced by co-transfecting HEK293T cells with the lentiviral metabolic library plasmids, psPAX2 (Addgene plasmid no. 12260) and pCAG4-Eco. At 48 h after transfection, virus was collected and frozen at −80 °C. Four hundred to five hundred million naive Cas9-expressing OT-I cells were isolated from 8–14 Cas9 OT-I mice and transduced at a multiplicity of infection of 0.3 to achieve about 20% transduction efficiency. After viral transduction, cells were cultured with human IL-2 (20 IU/ml; PeproTech), mouse IL-7 (2.5 ng/ml; PeproTech) and IL-15 (25 ng/ml; PeproTech) for 4 days to allow gene editing to occur. Transduced cells expressing ametrine were sorted using a Reflection cell sorter (iCyt), and an aliquot of 5×10^6 transduced OT-I cells was saved as input (about 500× cell coverage per sgRNA). Transduced OT-I cells (5×10^6 cells per recipient) were intravenously transferred into mice at day 14 after B16 Ova melanoma engraftment. Sixty recipients were randomly divided into three groups as biological replicates in each sub-library screening. At 7 days after adoptive transfer, transferred ametrine$^+$ OT-I cells were recovered from the tumour pooled from 20 recipients per sample using a Reflection cell sorter (iCyt). On average, 5×10^5 OT-I cells per sample (about 50× cell coverage per sgRNA) were recovered and used for deep sequencing of the sgRNA cassette, with the expectation that sgRNAs capable of improving ACT should be enriched in tumour-infiltrating OT-I cells.

Sequencing library preparation. Genomic DNA was extracted by using the DNeasy Blood & Tissue Kits (Qiagen 69506). Primary PCR was performed by using the KOD Hot Start DNA Polymerase (Millipore 71086) and the following pair of Nextera next-generation sequencing (NGS) primers (Nextera NGS forward (-F): TCGTCGGCAGCGTCAGATGTGTATAAGAGACAGttgtggaaaggacgaaacaccg; Nextera NGS reverse (-R): GTCTCGTGGGCTCGGAGATGTGTATAAGAGACAGccactttttcaagttgataacgg). Primary PCR products were purified using the AMPure XP beads (Beckman A63881). A second PCR was performed to add adaptors and indexes to each sample. Hi-seq 50-bp single-end sequencing (Illumina) was performed.

Data processing. For data analysis, FASTQ files obtained after sequencing were demultiplexed using the HiSeq Analysis software (Illumina). Single-end reads were trimmed and quality-filtered using the CLC Genomics Workbench v.11 (Qiagen) and matched against sgRNA sequences from the sgRNA metabolic library. Read counts for sgRNAs were normalized against total read counts across all samples. For each sgRNA, the fold change ($\log_2$-transformed ratio) for enrichment was calculated between each of the biological replicates and the input experiment. After merging the quantification results from two sub-libraries, candidate genes were ranked on the basis of the average enrichment of their six gene-specific sgRNAs in tumour-infiltrating OT-I cells relative to input ($\log_2$(TIL/input ratio); adjusted $P < 0.05$). The gene-level false-discovery-rate-adjusted *P* value was calculated among multiple sgRNAs ($n = 6$) of each gene, using a two-tailed paired Student's *t*-test between $\log_2$-transformed average normalized read counts of tumour

samples and those of input sample, and the *P* value was further adjusted using Bonferroni correction with gene size.

Genome-scale sgRNA Brie library CRISPR–Cas9 mutagenesis screening

In vivo screening. Lentivirus was produced by co-transfecting HEK293T cells with lentiviral genome-scale Brie library plasmids with the puromycin-resistance gene[28], psPAX2 and pCAG4-Eco. At 48 h after transfection, virus was collected and frozen at −80 °C. Two hundred million Cas9-expressing OT-I cells were isolated from 12 Cas9 OT-I mice and co-transduced with the Brie sgRNA library and *Regnase-1* sgRNA–ametrine. After viral transduction, cells were cultured with human IL-2 (20 IU/ml; PeproTech), mouse IL-7 (2.5 ng/ml; PeproTech) and IL-15 (25 ng/ml; PeproTech) for 2 days. Brie-sgRNA-library-transduced cells were then selected by culture with 4 μg/ml puromycin in the presence of the abovementioned cytokines for another 3 days. Following puromycin selection, ametrine$^+$ cells were sorted using a Relection cell sorter (iCyt) to select for cells cotransduced with sg*Renase-1* and Brie-library sgRNAs, and an aliquot of 10×10^6 transduced OT-I cells was saved as input (about 120× cell coverage per sgRNA). The majority of the co-transduced OT-I cells (5×10^6 cells per recipient) were then intravenously transferred into mice at day 14 after B16 Ova melanoma engraftment. Twenty recipients were randomly divided into two groups as biological replicates. At 7 days after adoptive transfer, transferred ametrine$^+$ OT-I cells were recovered from the tumour pooled from 10 recipients per sample using a Reflection cell sorter (iCyt). On average, 3×10^6 OT-I cells per sample (about 40× cell coverage per sgRNA) were recovered. DNA extraction and sequencing library preparation were as described in 'Sequencing library preparation'.

Data processing. For data analysis, FASTQ files obtained after sequencing were demultiplexed using the HiSeq Analysis software (Illumina). *Regnase-1* sgRNA (GGAGTGGAAACGCTTCATCG) reads were removed, and single-end reads were trimmed and quality-filtered using the CLC Genomics Workbench v.11 (Qiagen) and matched against sgRNA sequences from the genome-scale sgRNA Brie library. Read counts for sgRNAs were normalized against total read counts across all samples. For each sgRNA, the fold change ($\log_2$-transformed ratio) for enrichment was calculated between each of the biological replicates and the input experiment. Gene ranking was based on the average enrichment ($\log_2$(TIL/input ratio)) among replicates in representation of four individual corresponding sgRNAs in the genome-scale sgRNA Brie library. The gene-level false-discovery-rate-adjusted *P* value was calculated among multiple sgRNAs ($n = 4$) of each gene, using a using a two-tailed paired Student's *t*-test between $\log_2$-transformed average normalized read counts of tumour samples and those of the input sample, and the *P* value was further adjusted using Bonferroni correction with gene size.

Flow cytometry

For analysis of surface markers, cells were stained in PBS (Gibco) containing 2% (w/v) BSA (Sigma). Surface proteins were stained for 30 min on ice. Intracellular staining was performed with Foxp3/transcription factor staining buffer set, according to the manufacturer's instructions (eBioscience). Intracellular staining for cytokines was performed with a fixation/permeabilization kit (BD Biosciences). Active caspase-3 staining was performed using instructions and reagents from the Active Caspase-3 Apoptosis Kit (BD Biosciences). BrdU staining (pulsed for 18 h) was performed using instructions and reagents from the APC BrdU Flow Kit (BD Biosciences). 7-AAD (Sigma) or fixable viability dye (eBioscience) was used for dead-cell exclusion. The following antibodies were used: anti-IFNγ (XMG1.2), anti-TNF (MAb11), anti-IL-2 (JES6-5H4), anti-CD69 (H1.2F3), anti-CD25 (PC61.5), anti-KLRG1 (2F1), anti-ICOS (7E.17G9), anti-LAG3 (C9B7W), anti-PD-1 (J43), anti-CTLA4 (1B8), anti-TOX (TXRX10), anti-TIM3 (RMT3-23) (all from eBioscience); anti-GZMB (QA16A02), anti-CD49a (HMα1), anti-CD44 (IM7), anti-Ki-67 (16A8), anti-CD127 (A7R34) (all from Biolegend); anti-BrdU (3D4), anti-active caspase-3 (C92-605), anti-pH2A.X-S139 (N1-431) (DNA damage biomarker, which measures phosphorylation of the histone variant H2A.X at Ser139[46,47]), anti-SLAMF6 (13G3) (all from BD Biosciences); anti-BATF (D7C5), anti-TCF-1 (C63D9) (all from Cell Signaling Technology); anti-CD8α (53-6.7) (from SONY); and anti-CD62L (MEL-14) (from TONBO Bioscience). To monitor cell division, lymphocytes were labelled with CellTrace Violet (Life Technologies). For mitochondrial staining, lymphocytes were incubated for 30 min at 37 °C with 10 nM Mito Tracker Deep Red (Life Technologies) or 20 nM TMRM (ImmunoChemistry Technologies) after staining surface markers. Flow cytometry data were analysed using Flowjo 9.9.4 (Tree Star).

Adoptive T cell transfer for tumour therapy

B16 Ova cells (2×10^5) or B16 F10 cells (2×10^5) were injected subcutaneously into female C57BL/6 mice (7–10 weeks of age). At day 12, mice bearing tumours of a similar size were randomly divided into 3 groups (5–8 mice per group), and sgRNA-transduced OT-I cells (5×10^6) (for the treatment of B16 Ova melanomas) or pmel-1 (5×10^6) (for the treatment of B16 F10 melanomas) were injected intravenously. Tumours were measured every three days with digital callipers and tumour volumes were calculated by the formula: length × width × [(length × width)$^{0.5}$] × $\pi/6$ (ref. [48]). Death was defined as the point at which a progressively growing tumour reached 15 mm in the longest dimension. For the treatment of human CD19-Ph$^+$ B-ALL, mice engrafted with human CD19-Ph$^+$ B-ALL cells (1×10^6) were treated at day 7 with sgRNA-transduced CD8$^+$ CAR T cells (5×10^6). Mice were imaged using the Xenogen imaging system (Caliper Life Science).

TIL isolation

To isolate TILs, B16 Ova melanoma was excised, minced and digested with 0.5 mg/ml collagenase IV (Roche) + 200 IU/ml DNase I (Sigma) for 1 h at 37 °C, and then passed through 70-μm filters to remove undigested tumour tissues. TILs were then isolated by density-gradient centrifugation over Percoll (Life Technologies).

Gene expression profiling and GSEA

OT-I cells transduced with control sgRNA ($n = 4$ biological replicates) and *Regnase-1* sgRNA ($n = 5$ biological replicates) were isolated from the tumours or PLN of the hosts of the in vivo dual colour transfer assay, and analysed with RNA-seq. For RNA-seq, RNA was quantified using the Quant-iT RiboGreen assay (Life Technologies) and quality-checked by 2100 Bioanalyzer RNA 6000 Nano assay (Agilent) or LabChip RNA Pico Sensitivity assay (PerkinElmer) before library generation. Libraries were prepared from total RNA with the TruSeq Stranded Total RNA Library Prep Kit according to the manufacturer's instructions (Illumina, PN 20020595). Libraries were analysed for insert size distribution on a 2100 BioAnalyzer High Sensitivity kit (Agilent Technologies) or Caliper LabChip GX DNA High Sensitivity Reagent Kit (PerkinElmer). Libraries were quantified using the Quant-iT PicoGreen dsDNA assay (Life Technologies) or low-pass-sequencing with a MiSeq nano kit (Illumina). Paired-end 100-cycle sequencing was run on the HiSeq 4000 (Illumina). The raw reads were trimmed for adaptor sequences using Trimmomatic v.0.36 using parameters ILLUMINACLIP:adaptor.fa:2:30:10 LEADING:10 TRAILING:10 SLIDINGWINDOW:4:18 MINLEN:32, followed by mapping to the mm9 reference genome downloaded from gencode release M1 (https://www.gencodegenes.org/mouse/releases.html) using star v.2.5.2b. with default parameters. Reads were summarized at gene level using the Python script htseq-count. Differential expression analysis was performed using the R package DEseq2 v.1.18.1. OT-I cells transduced with *Regnase-1* sgRNA ($n = 3$ biological replicates) or *Batf* and *Regnase-1* sgRNAs ($n = 3$ biological replicates) were isolated from the tumours in the in vivo dual colour transfer assay and used for microarray analysis (Affymetrix Mouse Clariom S Assay). For microarray analysis, the expression signals were summarized using the

robust multi-array average algorithm Affymetrix Expression Console v.1.1, followed by differential expression analysis performed using the R package limma v.3.34.9. All the plots were generated using the R package ggplot2 v.2.2.1. Differentially expressed transcripts were identified using lmFit method implemented in limma v.3.34.9 and the Benjamini–Hochberg method was used to estimate the false discovery rate (FDR) as previously described[49]. Differentially expressed genes were defined by |fold change (log_2-transformed ratio)| > 0.5; Benjamini–Hochberg adjusted $P < 0.05$. GSEA was performed as previously described[50] using the 'Hallmark' database. For GSEA using manually curated gene signatures from public datasets, the microarray dataset (GSE84105)[12] was used for generating 'CXCR5$^+$ exhausted CD8 (Ahmed)' gene signatures (< 5% FDR); because the total number of upregulated and downregulated genes was more than 200, we ranked genes by their fold change (log_2-transformation of their expression in CXCR5$^+$ versus CXCR5$^-$) and used the top-200 upregulated genes as 'CXCR5$^+$ exhausted CD8 (Ahmed)'. RNA-seq data (GSE76279)[13] were processed using DEseq2 R package v.1.16.1 to generate 'CXCR5$^+$ exhausted CD8 (Yu)' using the same strategy.

ATAC-seq and data analysis

Library preparation. To prepare the ATAC-seq library, tumour-infiltrating sgRNA-transduced OT-I cells were collected in the following two batches: (a) control-sgRNA- and *Regnase-1*-sgRNA-transduced OT-I cells ($n = 4$ biological replicates per group) were isolated from tumour-bearing mice using the in vivo dual colour transfer assay; and (b) TIL OT-I cells transduced with control sgRNA, *Regnase-1* sgRNA, *Batf* sgRNA or *Batf* and *Regnase-1* sgRNAs ($n = 2$–4 replicates per group) were isolated from the tumour-bearing mice that received the individual transfer of sgRNA-transduced OT-I cells. Sorted T cells were incubated in 50 µl ATAC-seq lysis buffer (10 mM Tris-HCl, pH 7.4, 10 mM NaCl, 3 mM $MgCl_2$, 0.1% IGEPAL CA-630) on ice for 10 min. The resulting nuclei were pelleted at 500*g* for 10 min at 4 °C. The supernatant was carefully removed with a pipette and discarded. The pellet was resuspended in 50 µl transposase reaction mix (25 µl 2× TD buffer, 22.5 µl nuclease-free water and 2.5 µl transposase) and incubated for 30 min at 37 °C. After the reaction, the DNA was cleaned up using the Qiagen MinElute kit. The barcoding reaction was run using the NEBNext HiFi kit based on manufacturer's instructions, and amplified for 5 cycles according to a previous publication[20] and using the same primers. Ideal cycle numbers were determined from 5 µl (of 50 µl) from the previous reaction mix using KAPA SYBRFast (Kapa Biosystems) and a 20-cycle amplification on an Applied Biosystems 7900HT. Optimal cycles were determined from the linear part of the amplification curve and the remaining 45 µl of PCR reaction was amplified in the same reaction mix using the optimal cycle number.

Data analysis. ATAC-seq analysis was performed as previously described[51]. In brief, 2×100-bp paired-end reads obtained from all samples were trimming for Nextera adaptor by cutadapt (version 1.9, paired-end mode, default parameter with ' –m 6 –O 20') and aligned to mouse genome mm9 downloaded from gencode release M1 (https://www.gencodegenes.org/mouse/releases.html) by BWA (version 0.7.16, default parameters)[52], duplicated reads were then marked with Picard (version 2.9.4) and only non-duplicated proper paired reads have been kept by samtools (parameter '-q 1 -F 1804' version 1.9)[53]. After adjustment of Tn5 shift (reads were offset were offset by +4 bp for the sense strand and −5 bp for the antisense strand), we separated reads into nucleosome-free, mononucleosome, dinucleosome and trinucleosome (as previously described[20]) by fragment size and generated .bigwig files by using the centre 80-bp of fragments and scaled to 30×10^6 nucleosome-free reads. We observed reasonable nucleosome-free peaks and a pattern of mono-, di- and tri-nucleosomes on IGV (version 2.4.13)[54] and all 8 samples had about 10×10^6 nucleosome-free reads; we therefore concluded that the data qualities were good. Next, we merged each of the two replicates to enhance peak-calling on nucleosome-free reads by MACS2 (version 2.1.1.20160309 default parameters with '–extsize 200–nomodel')[55]. To assure replicability, we first finalized nucleosome-free regions for each genotype and retained a peak only if it called with a higher cutoff (macs2 -q 0.05) in one merged sample and at least called with a lower cutoff (macs2 -q 0.5) in the other merged sample. The reproducible peaks were further merged between wild-type and REGNASE-1-null samples and then we counted nucleosome-free reads from each of the eight samples using bedtools (v.2.24.0)[56]. To find the differentially accessible regions, we first normalized raw nucleosome-free read counts using the trimmed mean of *M*-values normalization method and applied an empirical Bayes statistics test after linear fitting using the voom package (R 3.23, edgeR 3.12.1, limma 3.26.9)[57]. FDR-corrected *P* value < 0.05 and fold change (log_2-transformed ratio) > 0.5 were used as cutoffs for more-accessible or less-accessible regions in REGNASE-1-null samples. We annotated the differentially accessible regions in ATAC-seq data for the nearest genes, and also superimposed these genes with 1,158 mitochondrial genes defined in the MitoCarta 2.0 database[58]. For motif analysis, we further selected regions < 0.05 fold change and *P* value > 0.5 as control regions. FIMO from MEME suite (version 4.11.3, '–thresh 1e-4–motif-pseudo 0.0001')[59] was used for scanning motif (TRANSFAC database, only included Vertebrata and not 3D structure-based) matches in the nucleosome-free regions and two-tailed Fisher's exact test was used to test whether a motif is significant enriched for differentially accessible regions compared to the control regions.

Footprinting of transcription-factor binding sites. Footprinting was performed as previously described[51]. In brief, we first generated .bigwig files according to all tags of adjusted reads, and then normalized them according to the number of autosome reads to 2×10^8 reads (for example, a sample with 1×10^8 autosome reads would be scaled so as to double the bigwig profile). We then generated average .bigwig files from the mean of replicates at each base pair for each sample, using motif matches within a nucleosome-free region for footprinting and taking the average profile across all motif matches at each base pair from −100 bp from motif match centres to +100 bp. Finally, the footprinting profiles were smoothed with 10-bp bins and plotted using deeptools (v.2.5.7)[60].

To identify the enrichment of BATF binding motifs, nucleosome-free differentially accessible regions were defined at |fold change (log_2-transformed ratio)| > 0.5; $P < 0.05$, and the peaks were further annotated as more- or less-accessible regions in REGNASE-1-null OT-I cells compared to wild-type controls. For each group, differentially accessible peaks were overlapped with BATF chromatin immunoprecipitation with sequencing (ChIP–seq) peaks (downloaded from GSE54191[26]) to identify the common regions between ATAC-seq peaks and BATF ChIP–seq peaks using bedtools (version 2.25.0). Finally, FIMO[61] from MEME suite (version 4.9.0) was used to scan the overlapping regions with TRANSFAC motifs associated with BATF to identify the number of motifs enriched in the differentially accessible regions in REGNASE-1-null (shown as '# Match (REGNASE-1-null)' in Extended Data Fig. 7d) or wild-type control samples (shown as '# Match (wild-type)' in Extended Data Fig. 7d), and Fisher's exact test was used to test the significance of enrichment. This statistical bioinformatics method has successfully been used to circumvent cell-number limitations[51,62].

Imaging

B16 Ova melanomas were fixed in PBS containing 2% PFA, 0.3% Triton-100 and 1% DMSO for 24 h before cryoprotection in 30% sucrose. Cryosections were blocked with 1% BSA and 0.05% Tween-20 in TBS (20 mM Tris, pH 8.0 and 100 mM NaCl) for 1 h at room temperature before overnight incubation in blocking buffer containing the following antibodies; anti-mCherry (Biorbyt orb11618), anti-GFP (Rockland Immuno 600-401-215), anti-TCF-7 (C63D9) (Cell Signaling Technology 2203)

and anti-TOM20 (2F8.1) (Millipore MABT166). Slides were washed in TBS before application of AF488, Cy3 or AF647 secondary antibodies (Jackson Immuno) for 1 h at room temperature before mounting with Prolong Diamond hardset medium containing DAPI (Thermo Fisher). Widefield fluorescence microscopy was performed using a motorized Nikon TiE inverted microscope equipped with a 20× Plan Apo 0.75 NA objective, standard DAPI, FITC and TRITC filter sets and an EMCCD camera (Andor). The entire tissue section was stitched on the basis of the DAPI fluorescent signal and the subsequent large images were analysed using NIS Elements software (Nikon Instruments). Images were segmented per channel, and further refined using a spot identification algorithm to identify single cells and positional information within the tumour. The number of cells per square area was determined following manual delineation of the tumour border. Analysis of transcription factor localization was performed using a Marianis spinning disk confocal microscope (Intelligent Imaging Innovations) equipped with a 100× 1.4 NA objective and Prime 95B sCMOS camera, and analysed using Slidebook software (Intelligent Imaging Innovations).

RNA isolation and real-time PCR

RNA was isolated using the RNeasy Micro Kit (Qiagen 74004) following the manufacturer's instructions. RNA was converted to cDNA using the High Capacity cDNA Reverse Transcription Kit (ThermoFisher 4368813) according to manufacturer's instructions. Real-time PCR was performed on the QuantStudio 7 Flex System (Applied Biosystems) using the PowerSYBR Green PCR Master Mix (ThermoFisher 4367659) and the following primers: *Irf4*-F: TCCGACAGTGGTTGATCGAC, *Irf4*-R: CCTCACGATTGTAGTCCTGCTT.

Protein extraction and immunoblot

Cells were lysed in RIPA buffer (ThermoFisher 89900), resolved in 4–12% Criterion XT Bis-Tris Protein Gel (Bio-Rad 3450124) and transferred to PVDF membrane (Bio-Rad 1620177). Membranes were blocked using 5% BSA for 1 h and then incubated for overnight with anti-MCPIP1 (604421) (R&D), anti-BATF (D7C5) (Cell Signaling Technology), anti-PTPN2 (E-11) (Santa Cruz Biotechnology), anti-SOCS1 (E-9) (Santa Cruz Biotechnology), anti-HSP90 (MAB3286) (R&D) or anti-β-actin (8H10D10) (Cell Signaling Technology) antibody. Membranes were washed 6 times with TBST and then incubated with 1:5,000 diluted HRP-conjugated anti-mouse IgG (W4021) (from Promega) for 1 h. Following another 6 washes with TBST, the membranes were imaged using the ODYSSEY Fc Analyzer (LI-COR).

Luciferase assay

The full-length 3′ UTR constructs of *Batf* (MmiT031430-MT06), *Il2* (MmiT092987-MT06) and *Il4* (MmiT092992-MT06) mRNAs were purchased from GeneCopoeia, each containing two luciferase genes: firefly luciferase gene for the 3′ UTR of the targeted gene, and the Renilla luciferase gene as an internal control. The cDNA of wild-type REGNASE-1 (Dharmacon MMM1013-202800061) was cloned into the pMIG-II vector. The D141N mutant of REGNASE-1 was generated by site-directed mutagenesis using the KOD Hot Start DNA Polymerase (Millipore 71086). HEK293T cells were transfected with the 3′ UTR construct of interest together with wild-type or the D141N mutant of REGNASE-1 expression plasmid, or empty control plasmid. At 48 h after transfection, cells were lysed and luciferase activities in the lysates were determined using the Luc-Pair Duo-Luciferase Assay Kit (GeneCopoeia LF002) according to manufacturer's instructions.

Seahorse metabolic assay

Oxygen consumption rates were measured in XF medium under basal conditions and in response to 1 μM oligomycin, 1.5 μM fluoro-carbonyl cyanide phenylhydrazone (FCCP) and 500 nM rotenone using an XF96 Extracellular Flux Analyzer (EFA) (Seahorse Bioscience).

scRNA-seq and data analysis

Library preparation. Control-sgRNA- and *Regnase-1*-sgRNA-transduced OT-I cells were sorted on a Reflection cell sorter (iCyt) from TILs pooled from the in vivo dual transfer hosts (6–8 mice per sample) at day 7 after adoptive transfer into tumour-bearing mice. The cells were counted and examined for viability using a Luna Dual Florescence Cell Counter (Logos Biosystems). All samples were spun down at 2,000 rpm for 5 min. The supernatant was removed, and cells were re-suspended in 100 μl of 1× PBS (Thermo Fisher Scientific) + 0.04% BSA (Amresco). The cells were then counted and examined for viability using a Luna Dual Florescence Cell Counter (Logos Biosystems). Cell counts were about 1×10^6 cells per millilitre and viability was above 98%. Single-cell suspensions were loaded onto the Chromium Controller according to their respective cell counts to generate 6,000 single-cell gel beads in emulsion per sample. Each sample was loaded into a separate channel. Libraries were prepared using the Chromium Single Cell 3′ v.2 Library and Gel Bead Kit (10X Genomics). The cDNA content of each sample after cDNA amplification of 12 cycles was quantified and quality-checked using a High-Sensitivity DNA chip with a 2100 Bioanalyzer (Agilent Technologies) to determine the number of PCR amplification cycles to yield a sufficient library for sequencing. After library quantification and quality-checking using DNA 1000 chip (Agilent Technologies), samples were diluted to 3.5 nM for loading onto the HiSeq 4000 (Illumina) with a 2 × 75-bp paired-end kit using the following read length: 26-bp read 1, 8-bp i7 index, and 98-bp read 2. An average of 400,000,000 reads per sample was obtained (approximately 80,000 reads per cell).

Alignment, barcode assignment and unique molecular identifier counting. The Cell Ranger 1.3 Single-Cell software suite (10X Genomics) was implemented to process the raw sequencing data from the Illumina HiSeq run. This pipeline performed demultiplexing, alignment (using the mouse genome mm10 from ENSEMBL GRCm38) and barcode processing to generate gene–cell matrices used for downstream analysis. Specifically, data from two control-sgRNA- and two *Regnase-1*-sgRNA-transduced TIL OT-I cell samples were combined into one dataset for consistent filtering, and unique molecular identifiers (UMIs) mapped to genes encoding ribosomal proteins were removed. Cells with low UMI counts (potentially dead cells with broken membranes) or high UMI counts (potentially two or more cells in a single droplet) were filtered. A small fraction of outlier cells (888) was further removed because of their low transcriptome diversity (meaning that fewer genes were detected than in other cells with a comparable number of captured UMIs). A total of 13,879 cells (control-sgRNA-transduced, 6,811; *Regnase-1*-sgRNA-transduced, 7,068) were captured, with an average of 11,040 mRNA molecules (UMIs, median: 9,391; range: 2,928–44,330). We normalized the expression level of each gene to 100,000 UMIs per cell and log-transformed them by adding 0.5 to the expression matrix.

Data visualization. Underlying cell variations derived from control-sgRNA- and *Regnase-1*-sgRNA-transduced TIL OT-I cell single-cell gene-expression data were visualized in a two-dimensional projection by *t*-SNE. Expression of individual genes or pathway scores was colour-coded (from low to high, blue–red) for each cell on *t*-SNE plots. To visualize *Tcf7*-expressing cells, we defined $Tcf7^{high}$ cells as cells with the highest third quantile of *Tcf7* expression (with $\log_2$(gene expression intensity) = 2.910317 as threshold) among all cells.

Statistical analysis for biological experiments

For biological experiment (non-omics) analyses, data were analysed using Prism 6 software (GraphPad) by two-tailed paired Student's *t*-test, two-tailed unpaired Student's *t*-test, or one-way ANOVA with Newman–Keuls's test. Two-way ANOVA was performed for comparing tumour

growth curves. The log-rank (Mantel–Cox) test was performed for comparing mouse survival curves. $P < 0.05$ was considered significant. Data are presented as mean ± s.d. or mean ± s.e.m.

Reporting summary

Further information on research design is available in the Nature Research Reporting Summary linked to this paper.

Data availability

Microarray, RNA-seq, ATAC-seq and scRNA-seq data have been deposited in the NCBI Gene Expression Omnibus (GEO) database and are accessible through the GEO SuperSeries accession number GSE126072. Source Data for Figs. 1–5 and Extended Data Figs. 1–9 are provided with the paper. All other relevant data are available from the corresponding author upon reasonable request.

40. Platt, R. J. et al. CRISPR–Cas9 knockin mice for genome editing and cancer modeling. *Cell* **159**, 440–455 (2014).
41. Hogquist, K. A. et al. T cell receptor antagonist peptides induce positive selection. *Cell* **76**, 17–27 (1994).
42. Overwijk, W. W. et al. Tumor regression and autoimmunity after reversal of a functionally tolerant state of self-reactive $CD8^+$ T cells. *J. Exp. Med*. **198**, 569–580 (2003).
43. Chen, R. et al. In vivo RNA interference screens identify regulators of antiviral $CD4^+$ and $CD8^+$ T cell differentiation. *Immunity* **41**, 325–338 (2014).
44. Birsoy, K. et al. An essential role of the mitochondrial electron transport chain in cell proliferation is to enable aspartate synthesis. *Cell* **162**, 540–551 (2015).
45. Sanson, K. R. et al. Optimized libraries for CRISPR–Cas9 genetic screens with multiple modalities. *Nat. Commun*. **9**, 5416 (2018).
46. Sukumar, M. et al. Mitochondrial membrane potential identifies cells with enhanced stemness for cellular therapy. *Cell Metab*. **23**, 63–76 (2016).
47. Wang, W. et al. Effector T cells abrogate stroma-mediated chemoresistance in ovarian cancer. *Cell* **165**, 1092–1105 (2016).
48. Wei, J. et al. Autophagy enforces functional integrity of regulatory T cells by coupling environmental cues and metabolic homeostasis. *Nat. Immunol*. **17**, 277–285 (2016).
49. Zeng, H. et al. mTORC1 couples immune signals and metabolic programming to establish T_{reg}-cell function. *Nature* **499**, 485–490 (2013).
50. Subramanian, A. et al. Gene set enrichment analysis: a knowledge-based approach for interpreting genome-wide expression profiles. *Proc. Natl Acad. Sci. USA* **102**, 15545–15550 (2005).
51. Karmaus, P. W. F. et al. Metabolic heterogeneity underlies reciprocal fates of T_H17 cell stemness and plasticity. *Nature* **565**, 101–105 (2019).
52. Li, H. & Durbin, R. Fast and accurate short read alignment with Burrows–Wheeler transform. *Bioinformatics* **25**, 1754–1760 (2009).
53. Li, H. et al. The Sequence Alignment/Map format and SAMtools. *Bioinformatics* **25**, 2078–2079 (2009).
54. Robinson, J. T. et al. Integrative genomics viewer. *Nat. Biotechnol*. **29**, 24–26 (2011).
55. Zhang, Y. et al. Model-based analysis of ChIP-seq (MACS). *Genome Biol*. **9**, R137 (2008).
56. Quinlan, A. R. & Hall, I. M. BEDTools: a flexible suite of utilities for comparing genomic features. *Bioinformatics* **26**, 841–842 (2010).
57. Law, C. W., Chen, Y., Shi, W. & Smyth, G. K. voom: precision weights unlock linear model analysis tools for RNA-seq read counts. *Genome Biol*. **15**, R29 (2014).
58. Calvo, S. E., Clauser, K. R. & Mootha, V. K. MitoCarta2.0: an updated inventory of mammalian mitochondrial proteins. *Nucleic Acids Res*. **44**, D1251–D1257 (2016).
59. Bailey, T. L. et al. MEME SUITE: tools for motif discovery and searching. *Nucleic Acids Res*. **37**, W202–W208 (2009).
60. Ramírez, F., Dündar, F., Diehl, S., Grüning, B. A. & Manke, T. deepTools: a flexible platform for exploring deep-sequencing data. *Nucleic Acids Res*. **42**, W187–W191 (2014).
61. Cuellar-Partida, G. et al. Epigenetic priors for identifying active transcription factor binding sites. *Bioinformatics* **28**, 56–62 (2012).
62. Krishnamoorthy, V. et al. The IRF4 gene regulatory module functions as a read-write integrator to dynamically coordinate T helper cell fate. *Immunity* **47**, 481–497 (2017).

Acknowledgements The authors acknowledge M. Hendren for animal colony management, C. Li for help with plasmids, G. Neale and S. Olsen for assistance with sequencing and St. Jude Immunology FACS core facility for cell sorting. This work was supported by NIH AI105887, AI131703, AI140761, AI150241, AI150514, and CA221290 (to H.C.).

Author contributions J.W. conceived the project, designed and performed in vitro and in vivo experiments, analysed data and wrote the manuscript; L.L. performed molecular experiments and analysed data; W.Z. performed CAR T-cell-related experiments and analysed data, with guidance from T.L.G., who also provided CAR transgenic mice and human CD19-Ph^+ B-ALL cell line; Y.D. performed bioinformatic analyses; S.A.L. helped to perform cellular experiments; C.G. performed imaging experiments; Y.W. performed Seahorse experiments; Y.-D.W. and J.Y. analysed CRISPR–Cas9 screening data; C.Q. performed scRNA-seq data analyses, with guidance from J.Y.; B.X. helped with ATAC-seq analysis; A.K. helped with molecular cloning; J.S. helped with ATAC-seq sample preparation; H.H. helped to perform scRNA-seq experiments; J.G.D. designed and generated the lentiviral sgRNA metabolic library and provided guidance for CRISPR–Cas9 screening data analyses; and H.C. helped to conceive and design experiments, co-wrote the manuscript and provided overall direction.

Competing interests H.C. and J.W. are authors of a patent application related to REGNASE-1 and BATF.

Additional information

Supplementary information is available for this paper at https://doi.org/10.1038/s41586-019-1821-z.

Correspondence and requests for materials should be addressed to H.C.

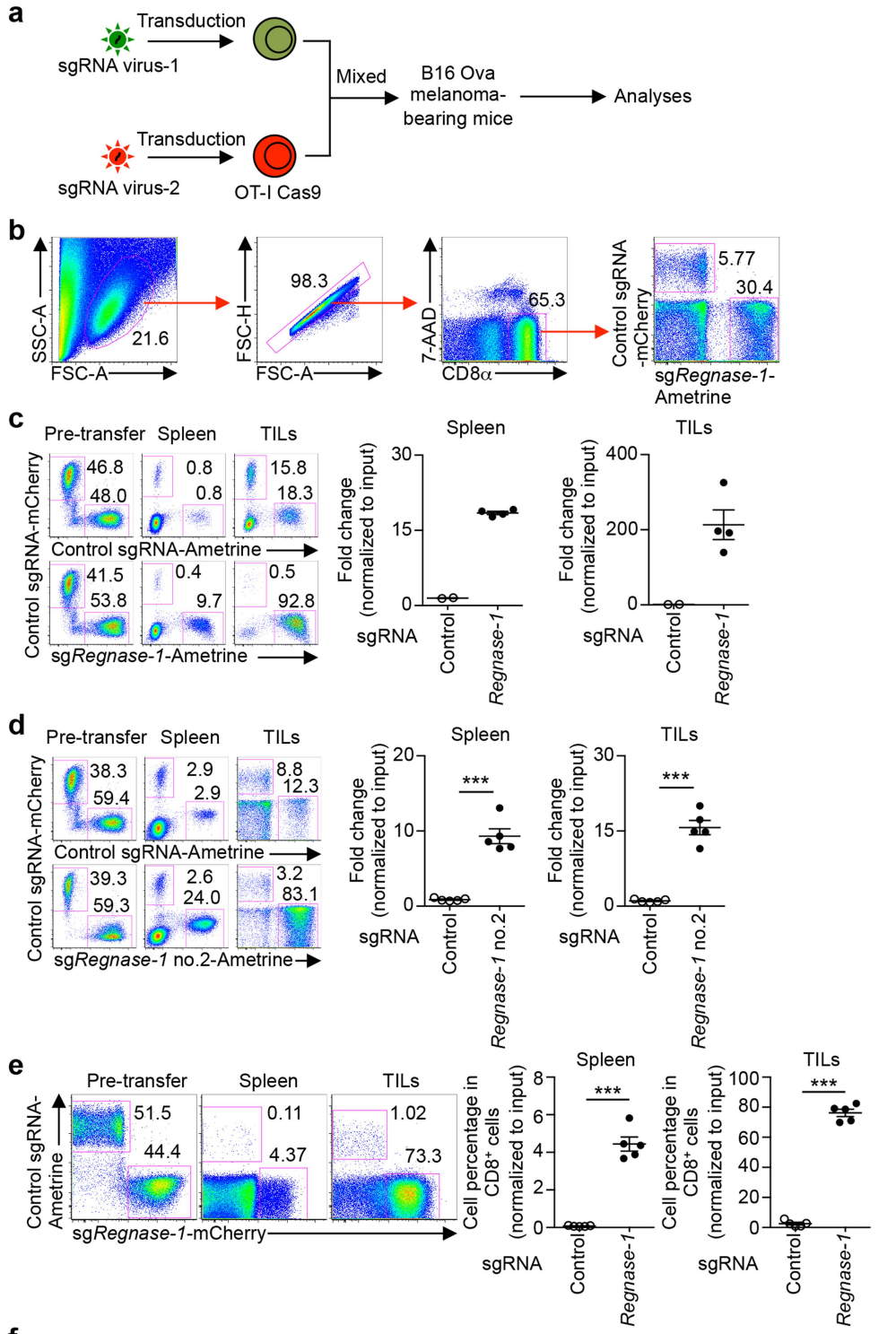

f

Sample	Total indel	#1-Indel	#1-Reads (%)	#2-Indel	#2-Reads (%)	#3-Indel	#3-Reads (%)
Control sgRNA	1.3%	-1	13 (1.1%)	1	1 (0.1%)	-2	1 (0.1%)
sg*Regnase-1*	97.3%	-1	309 (18.5%)	-19	116 (6.9%)	-4	113 (6.8%)

Extended Data Fig. 1 | See next page for caption.

Extended Data Fig. 1 | Validation of the effect of REGNASE-1 deletion on CD8$^+$ T cell accumulation in tumour immunity using the in vivo dual transfer system. a, Diagram of the in vivo dual transfer system. OT-I cells transduced with sgRNA viral vectors expressing distinct fluorescent proteins were mixed and transferred into the same tumour-bearing hosts, in which further analyses were performed. **b**, Gating strategy for sgRNA-transduced OT-I cell analysis. **c**, **d**, OT-I cells transduced with non-targeting control sgRNA (mCherry$^+$) were mixed at a 1:1 ratio with cells either transduced with control sgRNA (ametrine$^+$) (**c** ($n = 2$), **d** ($n = 5$), left, top) or two different sgRNAs targeting *Regnase-1* (*Regnase-1* sgRNA, ametrine$^+$, **c** ($n = 4$), left, bottom; or *Regnase-1* sgRNA no. 2, ametrine$^+$, **d** ($n = 5$), left, bottom), and transferred into tumour-bearing hosts. Mice were analysed at 7 days after adoptive transfer for the proportion of OT-I cells in CD8α$^+$ cells (**c**, **d**, left), and the quantification of relative OT-I cell percentages in CD8α$^+$ cells (normalized to input) in the spleen and TILs (**c**, **d**, right). Numbers in plots indicate the frequencies of OT-I cells. **e**, OT-I cells transduced with control sgRNA (ametrine$^+$) were mixed at a 1:1 ratio with cells transduced with *Regnase-1* sgRNA (mCherry$^+$) and transferred into tumour-bearing hosts ($n = 5$). Mice were analysed at 7 days after adoptive transfer for the proportion of OT-I cells in CD8α$^+$ cells (left), and the quantification of relative OT-I cell percentage in CD8α$^+$ cells (normalized to input) in the spleen and TILs (right). Numbers in plots indicate the frequencies of OT-I cells. **f**, Insertion and deletion (indel) mutations after CRISPR targeted disruption in OT-I cells transduced with either control sgRNA or *Regnase-1* sgRNA, via deep sequencing analysis of indels generated at the exonic target site of the *Regnase-1* gene, including 97.3% of indel events in *Regnase-1*-sgRNA-transduced cells isolated from tumours compared to 1.3% in control-sgRNA-transduced cells. Mean ± s.e.m. (**c**–**e**). ***$P < 0.001$. Two-tailed unpaired Student's *t*-test (**d**, **e**). Data are representative of two independent experiments (**e**).

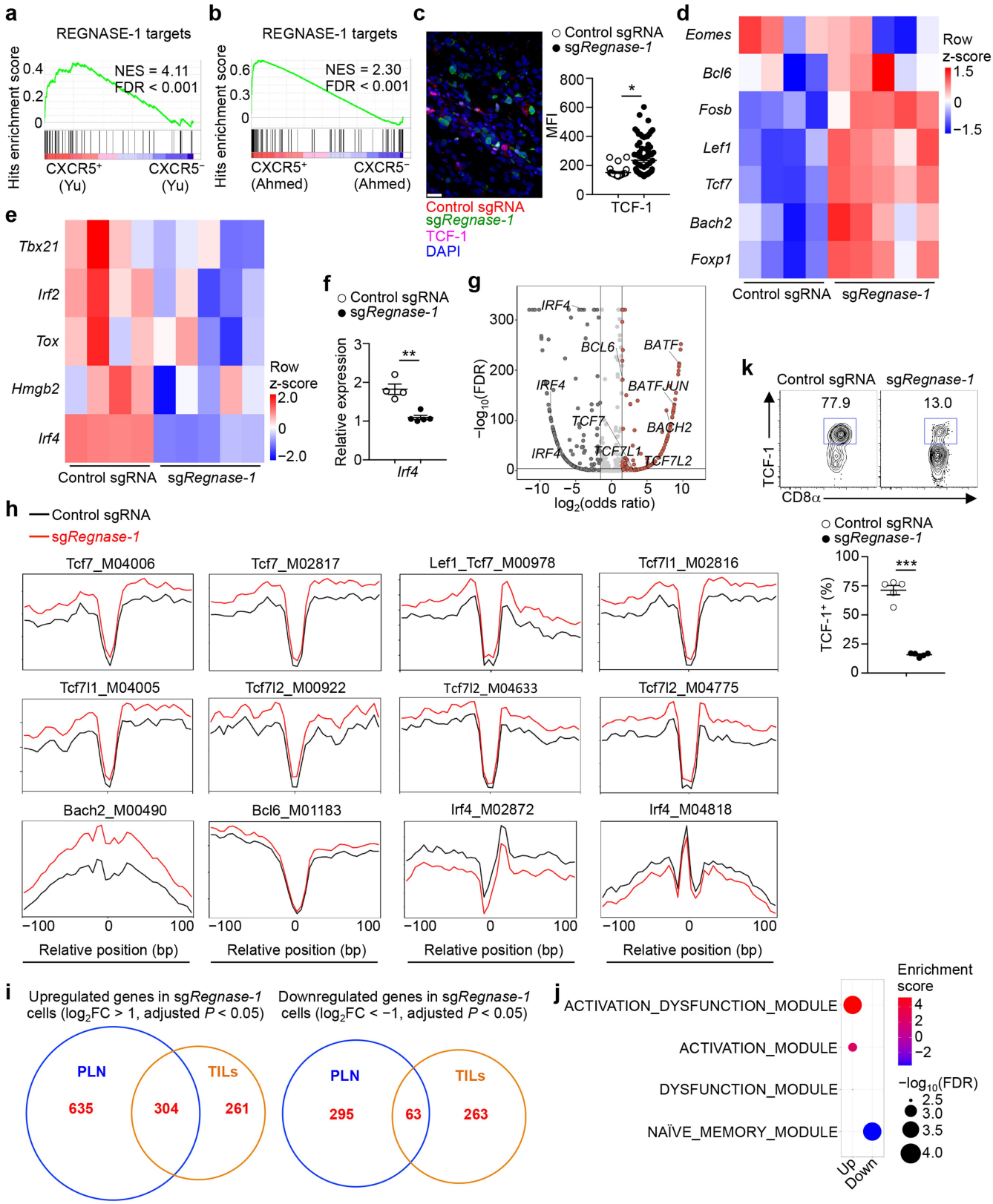

Extended Data Fig. 2 | See next page for caption.

Extended Data Fig. 2 | Tumour-infiltrating and peripheral REGNASE-1-null CD8$^+$ T cells show distinct immune signatures. a, **b**, GSEA enrichment plots of antigen-specific CXCR5$^+$ and CXCR5$^-$ exhausted CD8$^+$ T cells from chronic infection using gene targets repressed by REGNASE-1 (that is, the top 100 upregulated genes in TIL *Regnase-1*-sgRNA- compared to control-sgRNA-transduced OT-I cells, as identified using RNA-seq). **c**, Representative images (left) and quantification of MFI (right) of TCF-1 expression (pink) in control-sgRNA- (mCherry$^+$; red) and *Regnase-1*-sgRNA-transduced OT-I cells (ametrine$^+$; green) in the whole-tumour section ($n = 4$ mice). Scale bars, 20 μm. **d**, **e**, Gene-expression heat maps normalized by row (z-score) for the naive- or memory-T-cell-associated transcription factors (**d**) or effector- or exhausted-T-cell-associated transcription factors (**e**) in control-sgRNA- ($n = 4$) and *Regnase-1*-sgRNA ($n = 5$)-transduced OT-I cells isolated from TILs. Specifically, control-sgRNA- and *Regnase-1*-sgRNA-transduced OT-I cells were mixed and transferred into tumour-bearing mice, and tumour-infiltrating OT-I cells were isolated at day 7 for transcriptional profiling by RNA-seq. **f**, Real-time PCR analysis of *Irf4* mRNA expression in control-sgRNA- ($n = 4$ samples) and *Regnase-1*-sgRNA ($n = 5$ samples)-transduced OT-I cells isolated from TILs. **g**, Summary of ATAC-seq motif enrichment data showing $\log_2$(odds ratio) and $-\log_{10}$(FDR) of cells from control-sgRNA- and *Regnase-1*-sgRNA-transduced OT-I cells isolated from TILs ($n = 4$ samples per group). Specifically, control-sgRNA- and *Regnase-1*-sgRNA-transduced OT-I cells were mixed and transferred into tumour-bearing mice, and tumour-infiltrating OT-I cells were isolated at day 7 for ATAC-seq analysis. **h**, Tn5 insert sites from ATAC-seq analysis were aligned to motifs for transcription factors from the TRANSFAC database, and the binding profiles of TCF-1, BACH2, BCL6 and IRF4 are shown. **i**, Venn diagram showing the overlap of significantly upregulated (left, *Regnase-1*-sgRNA- ($n = 5$ samples) versus control-sgRNA-transduced OT-I cells ($n = 4$ samples)) or downregulated genes (right, *Regnase-1*-sgRNA- versus control-sgRNA-transduced OT-I cells) by RNA-seq profiling between TIL and PLN OT-I cells. Specifically, control-sgRNA- and *Regnase-1*-sgRNA-transduced OT-I cells were mixed and transferred into tumour-bearing mice, and OT-I cells were isolated at day 7 for transcriptional profiling by RNA-seq. **j**, GSEA enrichment plots of PLN *Regnase-1*-sgRNA- ($n = 5$) versus control-sgRNA ($n = 4$)-transduced OT-I cells using gene sets of four different tumour-infiltrating CD8 T cell activation states[11]. Specifically, control-sgRNA- and *Regnase-1*-sgRNA-transduced OT-I cells were mixed and transferred into tumour-bearing mice, and PLN OT-I cells were isolated at day 7 for transcriptional profiling by RNA-seq. **k**, OT-I cells transduced with control sgRNA (mCherry$^+$) and *Regnase-1* sgRNA (ametrine$^+$) were mixed and transferred into tumour-bearing mice ($n = 5$ mice), and OT-I cells in the spleen were analysed at day 7 for expression of TCF-1 (top), and quantification of the frequency of TCF-1$^+$ cells (bottom). Numbers in graphs indicate the frequencies of cells in gates. Mean ± s.e.m. (**c**, **f**, **k**). *$P < 0.05$, **$P < 0.01$, ***$P < 0.001$. Kolmogorov–Smirnov test followed by Benjamini–Hochberg correction (**a**, **b**, **j**), two-tailed unpaired Student's t-test (**c**, **f**, **k**), two-sided Fisher's exact test followed by Benjamini–Hochberg correction (**g**) or two-sided Fisher's exact test (**i**). Data are representative of two independent experiments (**c**, **f**, **k**).

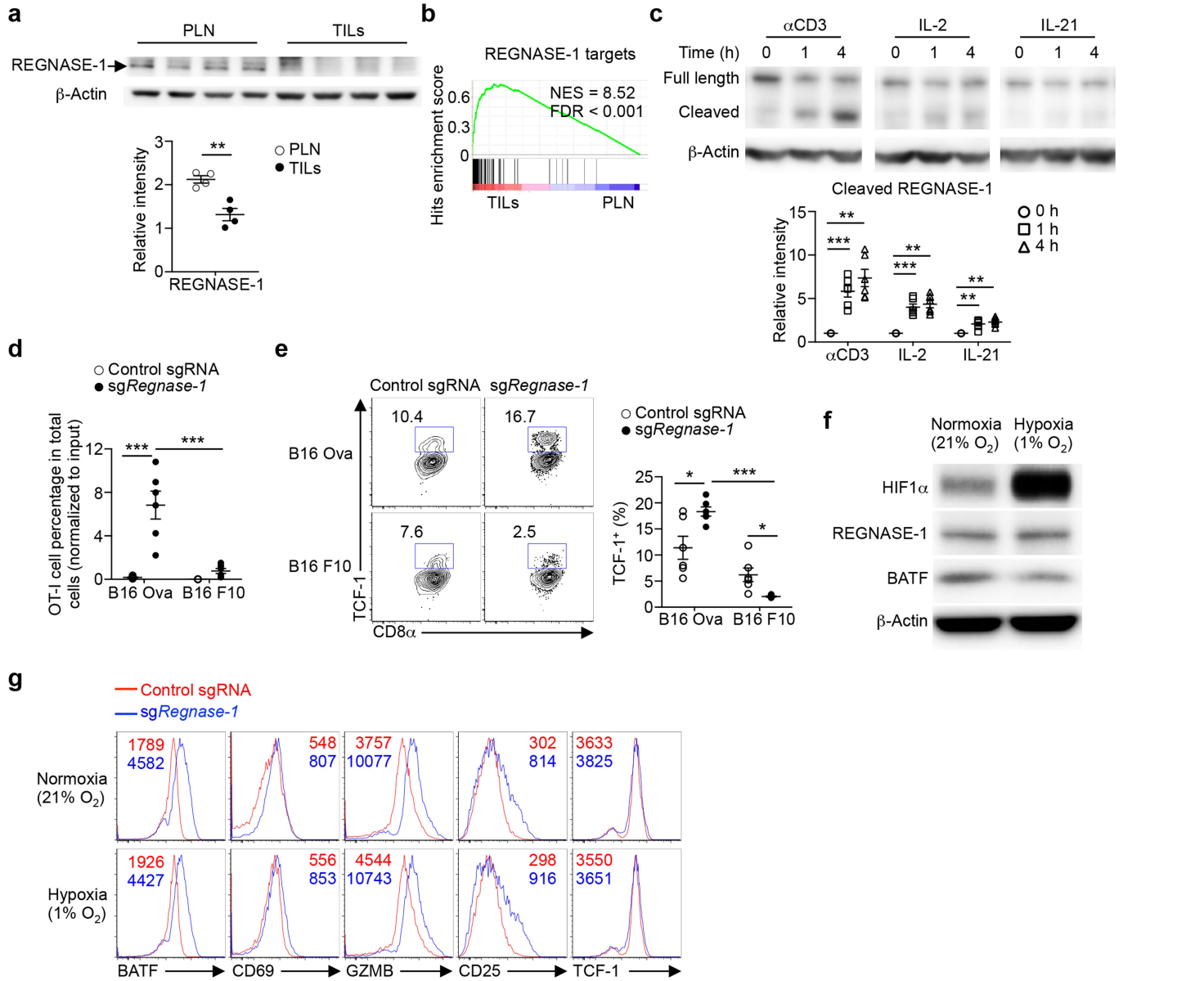

Extended Data Fig. 3 | Upstream signals regulate REGNASE-1 expression and REGNASE-1-null cell phenotypes. a, Immunoblot analysis of REGNASE-1 expression in control-sgRNA-transduced OT-I cells isolated from PLN and TILs at 7 days after adoptive transfer ($n = 4$ samples per group) (top). Quantification of the relative intensity of REGNASE-1 expression (bottom). β-Actin is used as a loading control. **b**, GSEA enrichment plots of PLN and TIL control-sgRNA-transduced OT-I cells ($n = 4$) used in **a**, by using gene targets repressed by REGNASE-1 (that is, the top 100 upregulated genes in TIL *Regnase-1*-sgRNA-compared to control-sgRNA-transduced cells, as identified using RNA-seq). **c**, OT-I cells were stimulated with anti-CD3 and anti-CD28 overnight before viral transduction, and then cultured in IL-7- and IL-15-containing medium for another 3 days in vitro. Pre-activated OT-I cells were then stimulated with anti-CD3, IL-2 or IL-21 for 0, 1 and 4 h ($n = 5$ samples per group) for immunoblot analysis of full-length and cleaved REGNASE-1 (top), and quantification of the relative intensity of cleaved REGNASE-1 expression (bottom). β-Actin is used as a loading control. **d**, **e**, OT-I cells transduced with control sgRNA (mCherry$^+$) and *Regnase-1* sgRNA (ametrine$^+$) were mixed at a 1:1 ratio and transferred into mice bearing B16 Ova ($n = 6$ mice) or B16 F10 ($n = 6$ mice) tumours. Mice were analysed at day 7 after adoptive transfer for quantification of relative OT-I cell percentage in total cells (normalized to input) in the TILs (**d**) and expression of TCF-1 (**e**, left), and quantification of the frequency of TCF-1$^+$ cells (**e**, right) in tumour-infiltrating OT-I cells. **f**, **g**, OT-I cells were stimulated with anti-CD3 and anti-CD28 overnight before viral transduction, and then cultured in IL-2-, IL-7- and IL-15-containing medium for another 3 days in vitro. Pre-activated OT-I cells were then continuously cultured in normoxia (21% O_2) or hypoxia (1% O_2) conditions for 48 h for immunoblot analysis of expression of HIF1α, REGNASE-1 and BATF (**f**), and for flow cytometry analysis of the expression of BATF, CD69, GZMB, CD25 and TCF-1 (**g**). Numbers in graphs indicate MFI (**g**). β-Actin is used as a loading control. Mean ± s.e.m. (**a**, **c**–**e**). $^*P < 0.05$, $^{**}P < 0.01$, $^{***}P < 0.001$. Two-tailed unpaired Student's *t*-test (**a**), Kolmogorov–Smirnov test followed by Benjamini–Hochberg correction (**b**) or one-way ANOVA (**c**–**e**). Data are representative of two (**c**, **f**, **g**) independent experiments, or pooled from two (**d**, **e**) independent experiments.

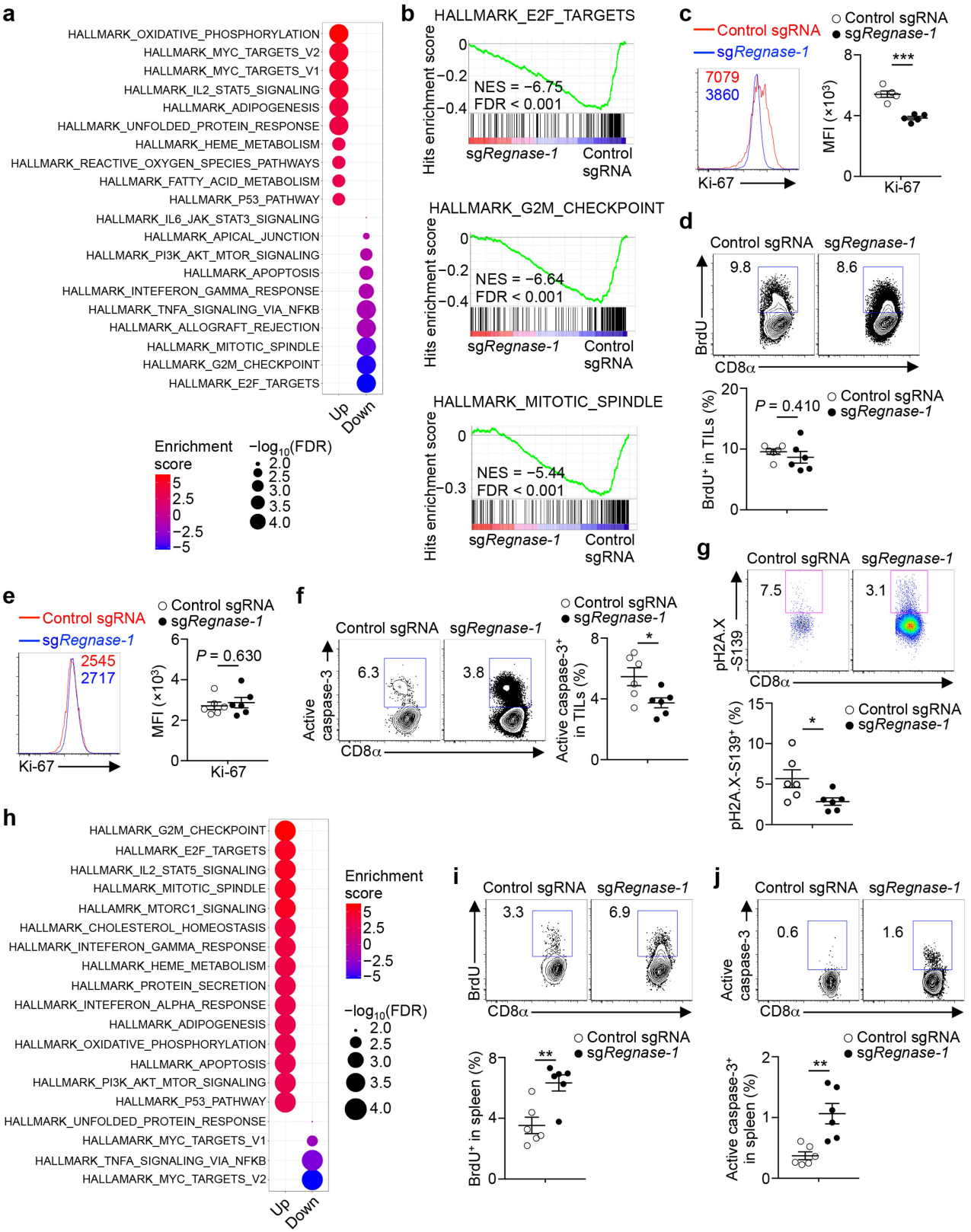

Extended Data Fig. 4 | See next page for caption.

Extended Data Fig. 4 | Proliferation and survival analyses of REGNASE-1-null CD8$^+$ T cells in tumour immunity. a, List of the top-10 significantly (FDR < 0.05) upregulated and downregulated pathways in TIL *Regnase-1*-sgRNA-transduced OT-I cells, as revealed by performing GSEA using Hallmark gene sets. Specifically, control-sgRNA- ($n = 4$) and *Regnase-1*-sgRNA ($n = 5$)-transduced OT-I cells were mixed and transferred into tumour-bearing mice, and tumour-infiltrating OT-I cells were isolated at day 7 for transcriptional profiling by RNA-seq. **b**, GSEA enrichment plots of TIL *Regnase-1*-sgRNA-transduced OT-I cells using cell-cycling-associated gene sets, including E2F targets (top), G2M checkpoint (middle) and mitotic spindle (bottom). **c**–**g**, OT-I cells transduced with control sgRNA (mCherry$^+$) and *Regnase-1* sgRNA (ametrine$^+$) were mixed and transferred into tumour-bearing mice, and tumour-infiltrating OT-I cells were analysed at day 7 (**d**–**g**) ($n = 6$ mice) and day 14 (**c**) ($n = 5$ mice) by flow cytometry for Ki-67 expression (**c**, left; **e**, left), BrdU incorporation (**d**, top; pulse for 18 h), active caspase-3 expression (**f**, left), Ser139 phosphorylation of histone variant H2A.X (**g**, top), and quantification of MFI of Ki-67 (**c**, right; **e**, right), frequency of BrdU$^+$ cells (**d**, bottom), frequency of active caspase-3$^+$ cells (**f**, right) and the frequency of the Ser139-phosphorylated histone variant H2A.X$^+$ cells (**g**, bottom). Numbers in graphs indicate the MFI of Ki-67 (**c**, left; **e**, left). Numbers in plots indicate the frequencies of BrdU$^+$ cells (**d**, top), active caspase-3$^+$ cells (**f**, left) and Ser139-phosphorylated histone variant H2A.X$^+$ cells (**g**, top). **h**, List of the top-15 significantly (FDR < 0.05) upregulated and top-4 significantly downregulated pathways in PLN *Regnase-1*-sgRNA-transduced OT-I cells, as revealed by performing GSEA using Hallmark gene sets. Specifically, control-sgRNA- ($n = 4$) and *Regnase-1*-sgRNA ($n = 5$)-transduced OT-I cells were mixed and transferred into tumour-bearing mice, and PLN OT-I cells were isolated at day 7 for transcriptional profiling by RNA-seq. **i**, **j**, OT-I cells transduced with control sgRNA (mCherry$^+$) and *Regnase-1* sgRNA (ametrine$^+$) were mixed and transferred into tumour-bearing mice, and OT-I cells in the spleen were analysed at day 7 (**i**, **j**) ($n = 6$ mice) by flow cytometry for BrdU incorporation (**i**, top; pulse for 18 h) and active caspase-3 expression (**j**, top), and quantification of frequencies of BrdU$^+$ cells (**i**, bottom) and active caspase-3$^+$ cells (**j**, bottom). Numbers in plots indicate the frequencies of BrdU$^+$ cells (**i**, top) and active caspase-3$^+$ cells (**j**, top). Mean ± s.e.m. (**c**–**g**, **i**, **j**). $^*P < 0.05$, $^{**}P < 0.01$, $^{***}P < 0.001$. Kolmogorov–Smirnov test followed by Benjamini–Hochberg correction (**a**, **b**, **h**) or two-tailed unpaired Student's *t*-test (**c**–**g**, **i**, **j**). Data are representative of two (**c**) independent experiments, or pooled from two (**d**–**g**, **i**, **j**) independent experiments.

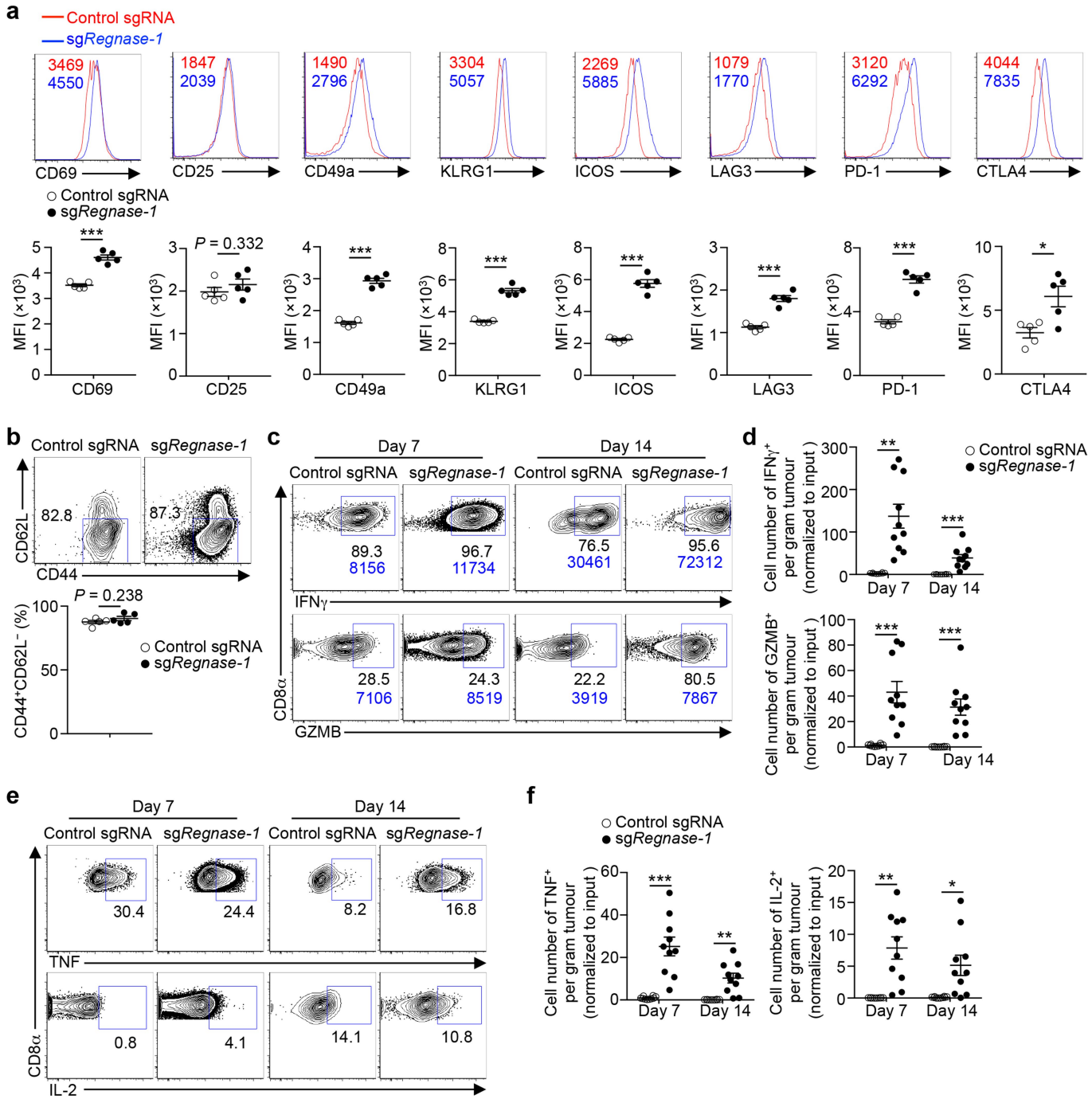

Extended Data Fig. 5 | Effector molecule expression of tumour-infiltrating REGNASE-1-null CD8⁺ T cells. a, **b**, OT-I cells transduced with control sgRNA (mCherry⁺) or *Regnase-1* sgRNA (ametrine⁺) were mixed at a 5:1 ratio and transferred into tumour-bearing mice ($n = 5$ mice), and tumour-infiltrating OT-I cells were analysed at day 7 for the expression of CD69, CD25, CD49a, KLRG1, ICOS, LAG3, PD-1 and CTLA4 (**a**, top) and CD44 and CD62L (**b**, top), and quantification of MFI of CD69, CD25, CD49a, KLRG1, ICOS, LAG3, PD-1 and CTLA4 (**a**, bottom) and frequency of CD44⁺CD62L⁻ cells (**b**, bottom). The numbers in graphs indicate the MFI (**a**, top). The numbers in plots indicate the frequency of CD44⁺CD62L⁻ cells (**b**, top). **c**–**f**, OT-I cells transduced with control sgRNA (mCherry⁺) or *Regnase-1* sgRNA (ametrine⁺) were mixed at a 5:1 ratio and transferred into tumour-bearing mice, and analysed at day 7 ($n = 10$ mice) or day 14 ($n = 10$ mice). Flow cytometry analysis of expression of IFNγ (**c**, top), GZMB (**c**, bottom), TNF (**e**, top) and IL-2 (**e**, bottom) in TIL OT-I cells, and quantification of the numbers of IFNγ⁺ cells (**d**, top), GZMB⁺ cells (**d**, bottom), TNF⁺ cells (**f**, left) and IL-2⁺ cells (**f**, right) per gram of tumour (normalized to input). The numbers adjacent to outlined areas indicate the frequencies of IFNγ⁺ cells and the MFI of IFNγ in IFNγ⁺ cells (**c**, top), and the frequency of GZMB⁺ cells and the MFI of GZMB in GZMB⁺ cells (**c**, bottom), and the frequencies of TNF⁺ cells (**e**, top) or IL-2⁺ cells (**e**, bottom). Mean ± s.e.m. (**a**, **b**, **d**, **f**). $^*P < 0.05$, $^{**}P < 0.01$, $^{***}P < 0.001$. Two-tailed unpaired Student's *t*-test (**a**, **b**) or two-tailed paired Student's *t*-test (**d**, **f**). Data are representative of two (**a**–**c**, **e**) independent experiments, or pooled from two (**d**, **f**) independent experiments.

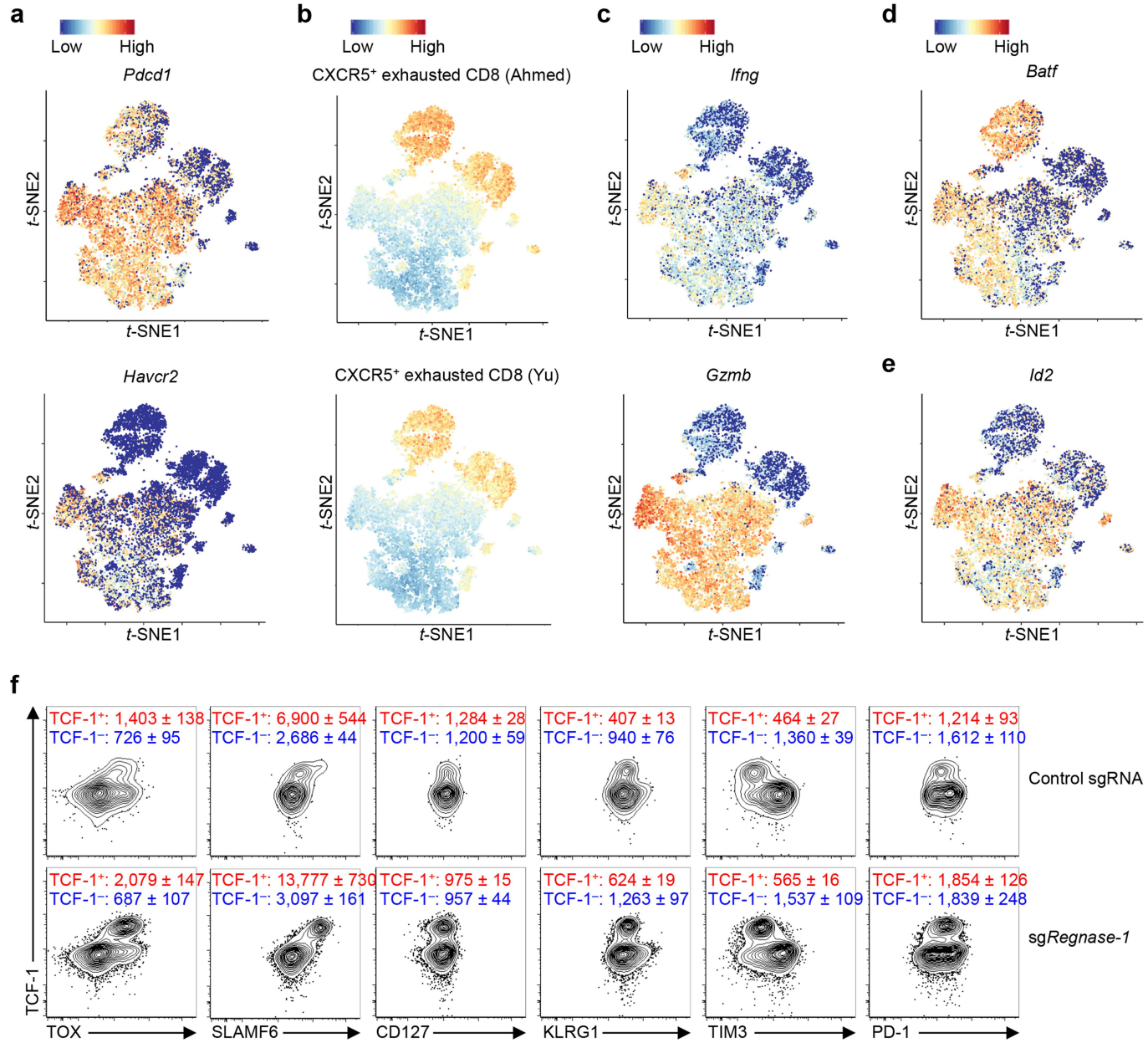

Extended Data Fig. 6 | scRNA-seq and flow cytometry analyses of tumour-infiltrating REGNASE-1-null OT-I cells. a–**e**, scRNA-seq analysis of control-sgRNA- and *Regnase-1*-sgRNA-transduced OT-I cells isolated from TILs. Specifically, control-sgRNA- and *Regnase-1*-sgRNA-transduced OT-I cells were mixed and transferred into tumour-bearing mice, and tumour-infiltrating OT-I cells were isolated at day 7 for transcriptional profiling by scRNA-seq. *t*-SNE visualization of *Pdcd1* (**a**, top), *Havcr2* (**a**, bottom), *Ifng* (**c**, top), *Gzmb* (**c**, bottom), *Batf* (**d**) and *Id2* (**e**) gene expression, and 'CXCR5$^+$ exhausted CD8 (Ahmed)[12]' (**b**, top) and 'CXCR5$^+$ exhausted CD8 (Yu)[13]' (**b**, bottom) gene signatures in individual cells. **f**, OT-I cells transduced with control sgRNA and *Regnase-1* sgRNA were mixed and transferred into tumour-bearing mice ($n = 5$ mice; data from 1 representative mouse are shown), and tumour-infiltrating OT-I cells were analysed at day 7 for the expression of TOX, SLAMF6, CD127, KLRG1, TIM3 and PD-1 in TCF-1$^+$ and TCF-1$^-$ cells of control-sgRNA- and *Regnase-1*-sgRNA-transduced OT-I cells. Numbers in graphs indicate the mean ± s.e.m. of MFI of markers on the *x*-axis after gating on TCF-1$^+$ or TCF-1$^-$ subsets. Data are representative of two independent experiments (**f**).

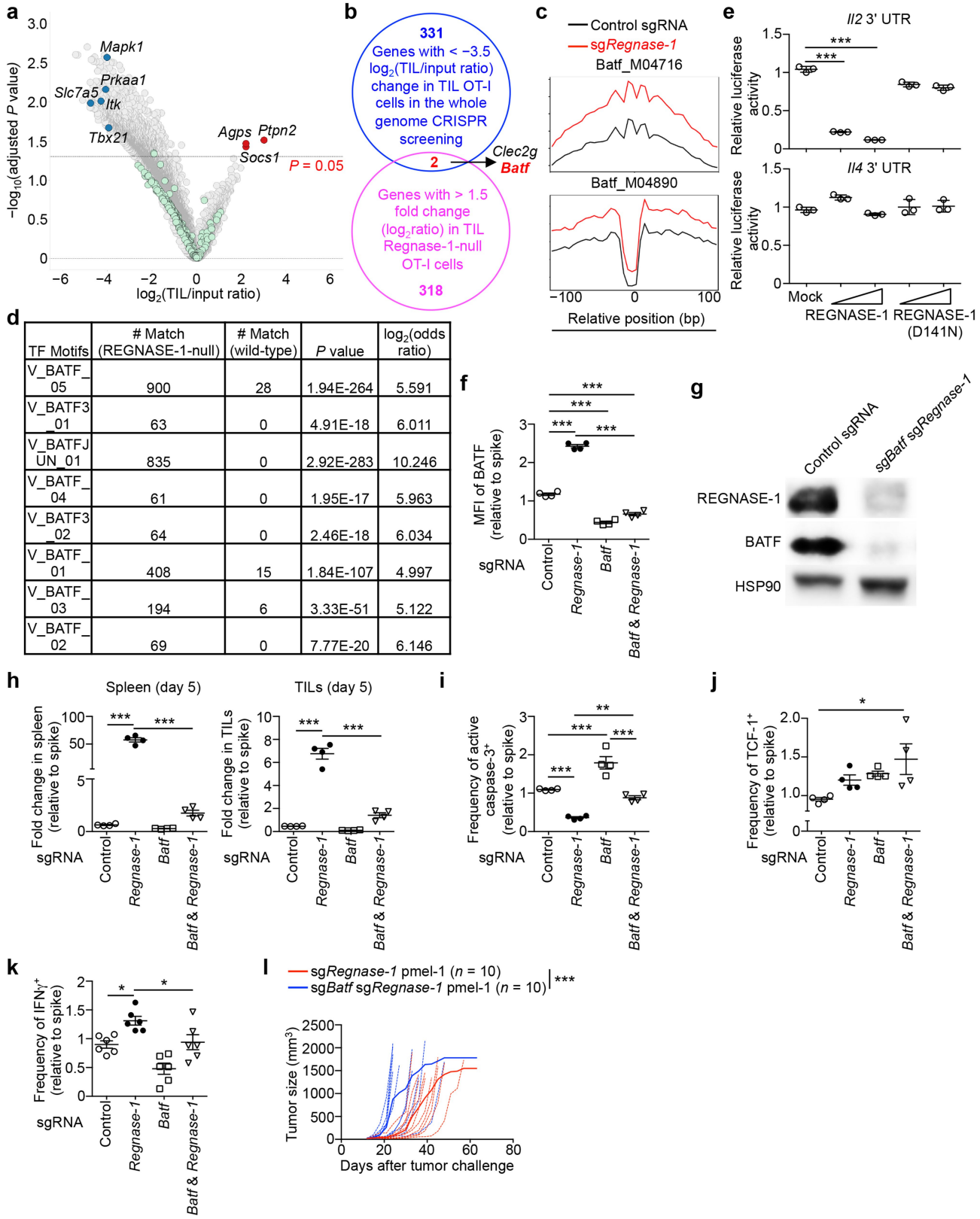

TF Motifs	# Match (REGNASE-1-null)	# Match (wild-type)	*P* value	$\log_2$(odds ratio)
V_BATF_05	900	28	1.94E-264	5.591
V_BATF3_01	63	0	4.91E-18	6.011
V_BATFJUN_01	835	0	2.92E-283	10.246
V_BATF_04	61	0	1.95E-17	5.963
V_BATF3_02	64	0	2.46E-18	6.034
V_BATF_01	408	15	1.84E-107	4.997
V_BATF_03	194	6	3.33E-51	5.122
V_BATF_02	69	0	7.77E-20	6.146

Extended Data Fig. 7 | See next page for caption.

Extended Data Fig. 7 | Genome-scale CRISPR screening identifies BATF as an important REGNASE-1 functional target in tumour immunity. a, Scatter plot of the enrichment of each gene versus its adjusted *P* value in genome-scale CRISPR screening. Gene enrichment was calculated by averaging the enrichment of the corresponding sgRNAs ($n = 4$ for each gene) in tumour-infiltrating OT-I cells relative to input ($\log_2$(TIL/input ratio)), with the most extensively enriched (red) and selectively depleted (blue) genes (adjusted $P < 0.05$), as well as dummy genes (green, generated by random combinations of 4 out of 1,000 non-targeting control sgRNAs per dummy gene). **b**, Venn diagram showing the overlap of genes between top-depleted genes in genome-scale CRISPR screening (by less than −3.5 $\log_2$(TIL/input ratio); adjusted $P < 0.05$) and top-upregulated genes in TIL *Regnase-1*-sgRNA- versus control-sgRNA-transduced OT-I cells as identified by RNA-seq (by greater than 1.5 fold change ($\log_2$-transformed ratio); adjusted $P < 0.05$). **c**, Tn5 insert sites from ATAC-seq analysis were aligned to motifs for transcription factors from the TRANSFAC database, and the binding profiles of BATF are shown. **d**, Enrichment of BATF-binding motifs in the genomic regions with upregulated accessibility in REGNASE-1-null cells. First, we analysed common regions in our REGNASE-1-null ATAC-seq data and published BATF ChIP-seq peaks (GSE54191[26]). Next, we scanned these common regions with TRANSFAC motifs for BATF, and numbers of motif matches and associated Fisher's exact test *P* values and $\log_2$(odds ratios) are shown (a positive $\log_2$(odds ratio) value indicates that a motif is more likely to occur in REGNASE-1-null cells than in wild-type samples; 'E−x' denotes '$\times 10^{-x}$'). **e**, Luciferase activity of HEK293T cells measured at 48 h after transfection with *Il2* mRNA 3′ UTR (top) or *Il4* mRNA 3′ UTR (bottom) luciferase reporter plasmid, together with control (mock), wild-type REGNASE-1- or REGNASE-1(D141N)-expressing plasmid ($n = 3$ samples per group). **f**, OT-I cells transduced with control sgRNA (mCherry$^+$; spike) were mixed at a 1:1 ratio with cells transduced with control sgRNA (ametrine$^+$), *Regnase-1* sgRNA (ametrine$^+$), *Batf* sgRNA (GFP$^+$) or *Batf* and *Regnase-1* sgRNAs (GFP$^+$ and ametrine$^+$), and transferred into tumour-bearing hosts individually ($n = 4$ mice per group). Mice were analysed at 5 days after adoptive transfer for quantification of relative MFI of BATF normalized to spike in the tumour-infiltrating OT-I cells (**f**). **g**, Immunoblot analysis of REGNASE-1 and BATF expression in in vitro cultured OT-I cells 3 days after transduction with control sgRNA or *Batf* and *Regnase-1* sgRNAs. HSP90 is used as a loading control. **h**–**k**, The same transfer system as in **f** was used. Five days after adoptive transfer, mice were analysed for the quantification of relative OT-I cell percentage in CD8α$^+$ cells normalized to spike in the spleen (**h**, left, $n = 4$) and TILs (**h**, right, $n = 4$). Tumour-infiltrating OT-I cells were analysed at day 5 ($n = 4$ mice per group) for the quantification of the relative frequency of active caspase-3$^+$ cells normalized to spike (**i**), and the quantification of the relative frequency of TCF-1$^+$ cells normalized to spike (**j**), or at day 7 ($n = 6$ mice per group) for quantification of the relative frequency of IFNγ$^+$ cells normalized to spike (**k**). **l**, Four million pmel-1 cells transduced with *Regnase-1* sgRNA (ametrine$^+$) ($n = 10$ recipients) or *Batf* and *Regnase-1* sgRNAs (GFP$^+$ and ametrine$^+$) ($n = 10$ recipients) were transferred into mice at day 12 after B16 F10 melanoma engraftment, followed by analysis of tumour size. Mean ± s.d. (**e**). Mean ± s.e.m. (**f**, **h**–**k**). $^*P < 0.05$, $^{**}P < 0.01$, $^{***}P < 0.001$. Two-tailed unpaired Student's paired *t*-test followed by Bonferroni correction (**a**), two-sided Fisher's exact test (**d**), one-way ANOVA (**e**, **f**, **h**–**k**) or two-way ANOVA (**l**). Data are representative of two (**e**) or three (**g**) independent experiments, or pooled from two (**f**, **h**–**l**) independent experiments.

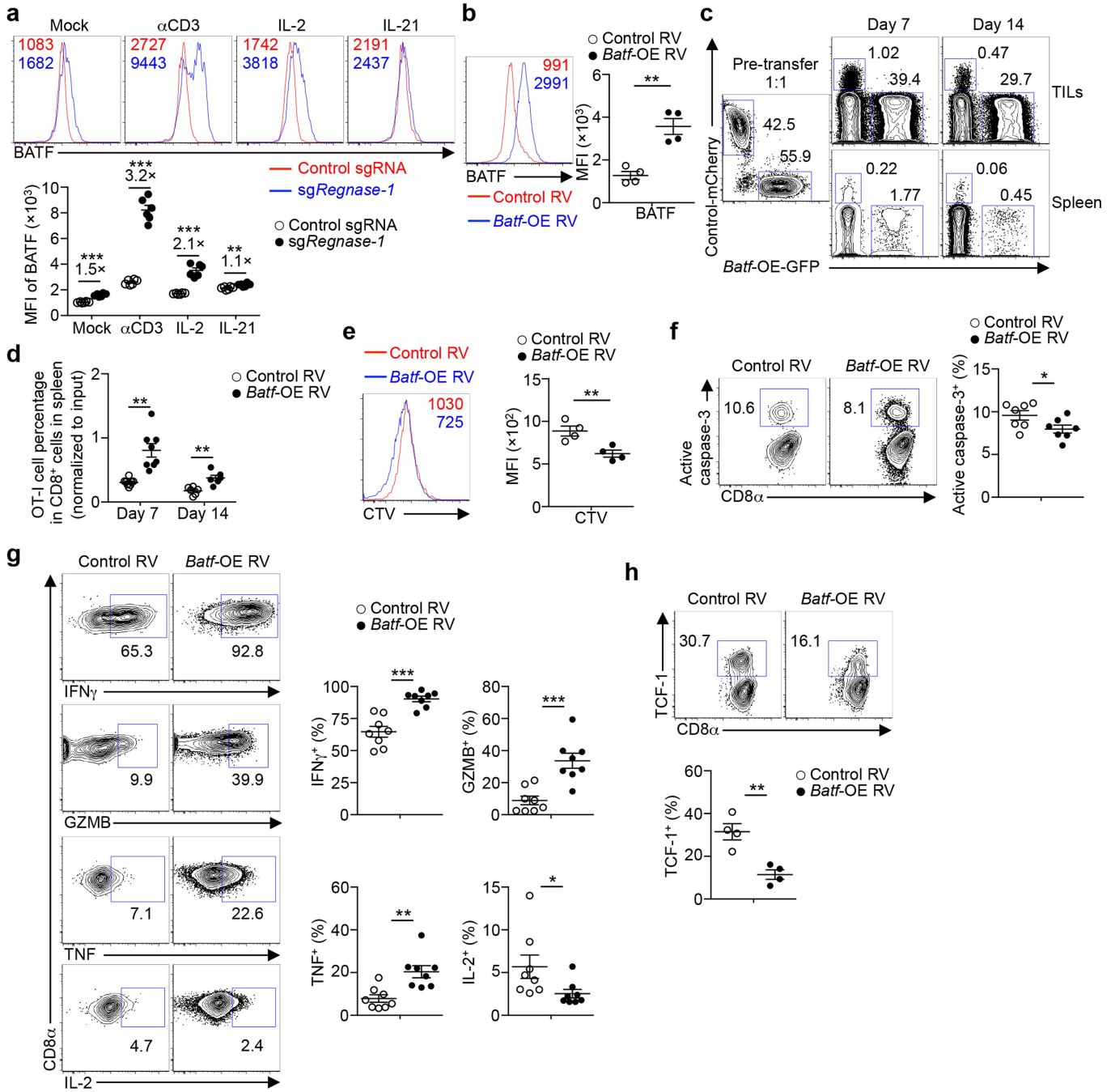

Extended Data Fig. 8 | BATF overexpression markedly enhances CD8⁺ T cell antitumour responses. a, OT-I cells were stimulated with anti-CD3 and anti-CD28 overnight before viral transduction, and then cultured in IL-7- and IL-15-containing medium for another 3 days in vitro. Control-sgRNA- and *Regnase-1*-sgRNA-transduced OT-I cells were then stimulated with anti-CD3, IL-2 or IL-21 overnight for flow cytometry analysis of BATF expression (top), and quantification of the MFI of BATF (bottom) ($n = 6$ samples per group). Numbers in graphs indicate the MFI (top) and fold change between comparisons (bottom). **b**–**h**, OT-I cells transduced with control retrovirus (RV; mCherry⁺) were mixed at a 1:1 ratio with cells transduced with *Batf*-overexpressing retrovirus (GFP⁺), and transferred into tumour-bearing hosts. Mice were analysed at day 4 (**e**) ($n = 4$ mice), day 5 (**b**, **h**) ($n = 4$ mice), day 7 (**c**, **d**, **f**, **g**) ($n = 6$–8 mice) or day 14 (**c**, **d**) ($n = 6$ mice) for the expression of BATF (**b**, left), active caspase-3 (**f**, left), IFNγ, GZMB, TNF and IL-2 (**g**, left) and TCF-1 (**h**, top) in TIL OT-I cells; the quantification of the MFI of BATF in TIL OT-I cells (**b**, right); quantification of the frequencies of active caspase-3⁺ cells (**f**, right), IFNγ⁺, GZMB⁺, TNF⁺ and IL-2⁺ cells (**g**, right) and TCF-1⁺ cells (**h**, bottom) in TIL OT-I cells; analysis of the proportion of donor-derived OT-I cells in total CD8α⁺ cells in TILs and spleen (**c**); the quantification of the relative OT-I cell percentage in CD8α⁺ cells in the spleen (normalized to input) (**d**); the dilution of CellTrace Violet (CTV) in TIL OT-I cells (**e**, left); and the quantification of the MFI of CTV in TIL OT-I cells (**e**, right). The numbers in graphs indicate the MFI (**b**, left; **e**, left), the frequencies of OT-I cells in gates (**c**), the frequency of active caspase-3⁺ cells (**f**, left), the frequencies of IFNγ⁺, GZMB⁺, TNF⁺ or IL-2⁺ cells (**g**, left), and the frequency of TCF-1⁺ cells (**h**, top). Mean ± s.e.m. (**a**, **b**, **d**–**h**). $^{*}P < 0.05$, $^{**}P < 0.01$, $^{***}P < 0.001$. Two-tailed unpaired Student's *t*-test (**a**, **b**, **d**–**h**). Data are representative of two (**a**, **c**) independent experiments, or pooled from two (**b**, **d**–**h**) independent experiments.

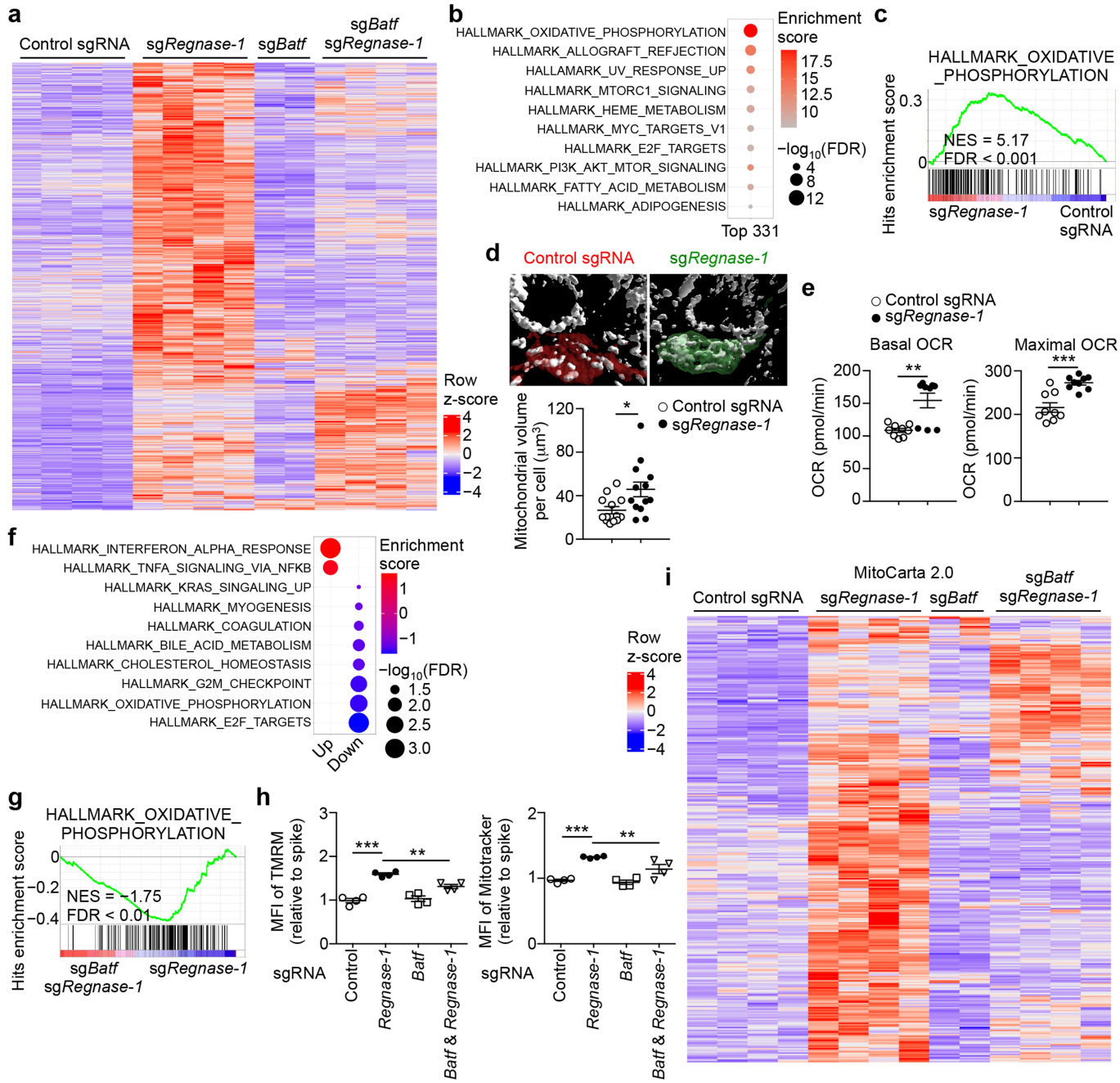

Extended Data Fig. 9 | See next page for caption.

Extended Data Fig. 9 | Genome-scale CRISPR screening identifies mitochondrial metabolism as an important downstream pathway of REGNASE-1 and BATF. a, Chromatin accessibility heat maps normalized by row (*z*-score) for 7,480 genes with significantly increased chromatin accessibility (by |fold change (log_2-transformed ratio)| > 0.5; $P < 0.05$) in *Regnase-1*-sgRNA-transduced OT-I cells as compared to control-sgRNA-transduced cells. Specifically, OT-I cells transduced with control sgRNA (mCherry$^+$) ($n = 4$), *Regnase-1* sgRNA (ametrine$^+$) ($n = 4$), *Batf* sgRNA (GFP$^+$) ($n = 2$) or *Batf* and *Regnase-1* sgRNAs (GFP$^+$ and ametrine$^+$) ($n = 4$) were transferred into tumour-bearing hosts individually. OT-I cells were isolated from TILs at day 7 for ATAC-seq analysis. We annotated the differential accessibility regions in ATAC-seq for the nearest genes, and identified 7,480 genes with significantly increased chromatin accessibility in REGNASE-1-null cells as compared to wild-type cells. BATF co-deletion reversed the upregulated chromatin accessibility for a large proportion of these genes (5,052 in total). Also, 2,527 of these 5,052 genes showed significantly downregulated chromatin accessibility in BATF-null cells as compared to wild-type cells. **b**, Functional enrichment plots of the top-10 significantly (FDR < 0.05) enriched pathways in top-ranking depleted genes ($n = 4$ sgRNAs for each gene) identified in the genome-scale CRISPR screening (by less than −3.5 log_2(TIL/input ratio); adjusted $P < 0.05$). **c**, GSEA enrichment plots of TIL *Regnase-1*-sgRNA-transduced OT-I cells using the OXPHOS Hallmark gene set. Specifically, control-sgRNA- and *Regnase-1*-sgRNA-transduced OT-I cells were mixed and transferred into tumour-bearing mice, and tumour-infiltrating OT-I cells were isolated at day 7 for transcriptional profiling by RNA-seq. **d**, Representative images (top) and quantification of mitochondrial volume (stained with TOM20, white) per cell (bottom) in control-sgRNA- (mCherry$^+$; red) and *Regnase-1*-sgRNA-transduced OT-I cells (ametrine$^+$; green) in tumours at 7 days after adoptive transfer ($n = 4$ mice). **e**, Oxygen consumption rate (OCR) bioenergetic profiling of control-sgRNA- and *Regnase-1*-sgRNA-transduced OT-I cells cultured in vitro for basal (left) and maximal (right) OCR ($n = 9$ samples per group). **f**, List of the top-2 significantly (FDR < 0.05) upregulated and top-8 significantly downregulated pathways in TIL *Batf*-and-*Regnase-1*-sgRNAs- versus *Regnase-1*-sgRNA-transduced OT-I cells ($n = 3$ samples per group) isolated from TILs, as revealed by performing GSEA using the Hallmark gene sets. Specifically, *Regnase-1*-sgRNA- and *Batf*-and-*Regnase-1*-sgRNA-transduced OT-I cells were mixed and transferred into tumour-bearing mice, and tumour-infiltrating OT-I cells were isolated at day 7 for transcriptional profiling by microarray. **g**, GSEA enrichment plots of TIL *Batf*-and-*Regnase-1*-sgRNAs- versus *Regnase-1*-sgRNA-transduced OT-I cells ($n = 3$ samples per group) using the OXPHOS gene set. **h**, OT-I cells transduced with control sgRNA (mCherry$^+$; spike) were mixed at a 1:1 ratio with cells transduced with control sgRNA (ametrine$^+$), *Regnase-1* sgRNA (ametrine$^+$), *Batf* sgRNA (GFP$^+$) or *Batf* and *Regnase-1* sgRNA (GFP$^+$ and ametrine$^+$), and transferred into tumour-bearing hosts individually ($n = 4$ mice per group). Mice were analysed at 5 days after adoptive transfer for quantification of the relative MFI of TMRM (left) and Mitotracker (right), normalized to spike in tumour-infiltrating OT-I cells. **i**, Chromatin accessibility heat maps normalized by row (*z*-score) for mitochondrial genes with significantly increased chromatin accessibility (by |fold change (log_2-transformed ratio)| > 0.5; $P < 0.05$) in *Regnase-1*-sgRNA-transduced OT-I cells compared to control-sgRNA-transduced cells, determined by ATAC-seq as described in **a**. We annotated the differential accessibility regions in ATAC-seq for the nearest genes, and superimposed these genes with 1,158 mitochondrial genes defined in the MitoCarta 2.0 database. A total of 341 mitochondrial genes showed significantly upregulated chromatin accessibility in the absence of REGNASE-1, 214 of which were blocked by BATF co-deletion in BATF-null REGNASE-1-null cells. Moreover, 96 of these 214 genes showed significantly downregulated chromatin accessibility in BATF-null cells as compared to wild-type cells. Mean ± s.e.m. (**d**, **e**, **h**). $^*P < 0.05$, $^{**}P < 0.01$, $^{***}P < 0.001$. Two-sided Fisher's exact test (**a**, **i**), right-tailed Fisher's exact test (**b**), Kolmogorov–Smirnov test followed by Benjamini–Hochberg correction (**c**, **f**, **g**), two-tailed unpaired Student's *t*-test (**d**, **e**) or one-way ANOVA (**h**). Data are representative of two (**d**, **e**) independent experiments, or pooled from two (**h**) independent experiments.

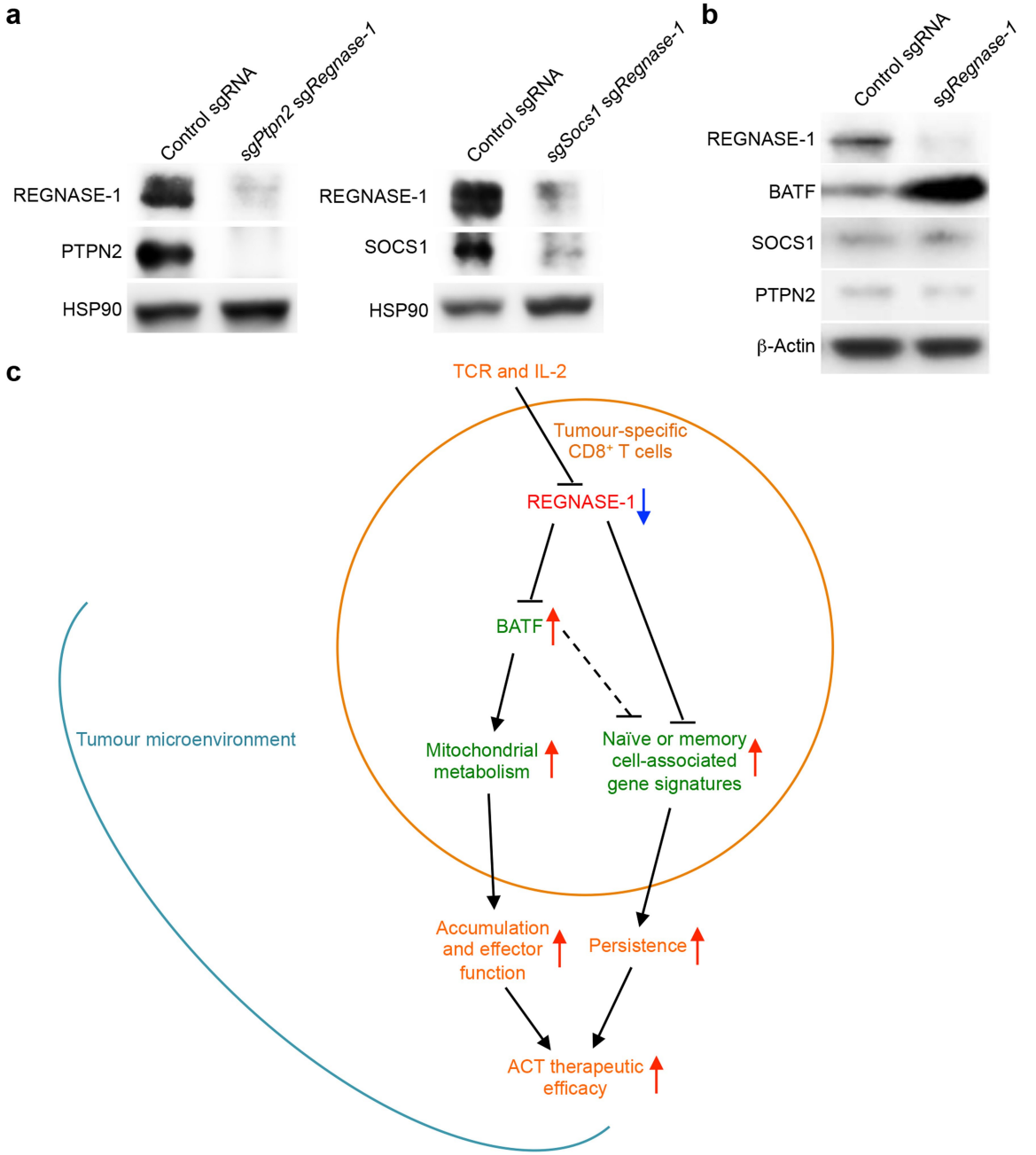

Extended Data Fig. 10 | Targeting PTPN2 and SOCS1 and model of REGNASE-1 functions in tumour-specific CD8$^+$ T cells. a, Immunoblot analysis of REGNASE-1, PTPN2 and SOCS1 expression in OT-I cells cultured in vitro, 3 days after transduction with control sgRNA, *Ptpn2* and *Regnase-1* sgRNAs (left) or *Socs1* and *Regnase-1* sgRNAs (right). HSP90 is used as a loading control. **b**, Immunoblot analysis of REGNASE-1, BATF, SOCS1 and PTPN2 expression in OT-I cells transduced with control sgRNA or *Regnase-1* sgRNA, cultured in vitro for 3 days after viral transduction. β-Actin is used as a loading control. **c**, REGNASE-1 is a major negative regulator of CD8$^+$ T cell antitumour responses, and TCR and IL-2 inhibit its expression and activity. Deletion of REGNASE-1 unleashes a potent therapeutic efficacy of engineered tumour-specific CD8$^+$ T cells against cancers, by coordinating transcriptional and metabolic programs to achieve greatly improved cell accumulation and function. As a key functional target of REGNASE-1, excessive BATF drives robust cell accumulation and effector function—in part through enhancing mitochondrial metabolism—in REGNASE-1-null CD8$^+$ T cells. REGNASE-1 deletion also reprograms cells to acquire increased gene signatures associated with naive or memory cells and to gain survival advantage, which contribute to the improved persistence of REGNASE-1-null effector CD8$^+$ T cells. Targeting PTPN2 and SOCS1 (not depicted here) acts in coordination with REGNASE-1 inhibition to promote CD8$^+$ T cell antitumour responses. Data are representative of three independent experiments (**a**, **b**).

nature research

Corresponding author(s): Hongbo Chi

Last updated by author(s): Oct 24, 2019

Reporting Summary

Nature Research wishes to improve the reproducibility of the work that we publish. This form provides structure for consistency and transparency in reporting. For further information on Nature Research policies, see Authors & Referees and the Editorial Policy Checklist.

Statistics

For all statistical analyses, confirm that the following items are present in the figure legend, table legend, main text, or Methods section.

n/a	Confirmed	
☐	☒	The exact sample size (*n*) for each experimental group/condition, given as a discrete number and unit of measurement
☐	☒	A statement on whether measurements were taken from distinct samples or whether the same sample was measured repeatedly
☐	☒	The statistical test(s) used AND whether they are one- or two-sided *Only common tests should be described solely by name; describe more complex techniques in the Methods section.*
☐	☒	A description of all covariates tested
☐	☒	A description of any assumptions or corrections, such as tests of normality and adjustment for multiple comparisons
☐	☒	A full description of the statistical parameters including central tendency (e.g. means) or other basic estimates (e.g. regression coefficient) AND variation (e.g. standard deviation) or associated estimates of uncertainty (e.g. confidence intervals)
☐	☒	For null hypothesis testing, the test statistic (e.g. *F*, *t*, *r*) with confidence intervals, effect sizes, degrees of freedom and *P* value noted *Give P values as exact values whenever suitable.*
☒	☐	For Bayesian analysis, information on the choice of priors and Markov chain Monte Carlo settings
☒	☐	For hierarchical and complex designs, identification of the appropriate level for tests and full reporting of outcomes
☒	☐	Estimates of effect sizes (e.g. Cohen's *d*, Pearson's *r*), indicating how they were calculated

Our web collection on statistics for biologists contains articles on many of the points above.

Software and code

Policy information about availability of computer code

Data collection	No software was used.
Data analysis	Flowjo 9.9.4 (Tree Star) for FACS results; GraphPad Prism 6 for statistics; CLC Genomics Workbench v11 (Qiagen) for Hi-seq FastQ file analysis; Trimmomatic v.0.36, star v.2.5.2b and R package DEseq2 v. 1.18.1 for RNA-seq analysis; Affymetrix Expression Console v.1.1, R package limma v.3.34.9, R package ggplot2 v.2.2.1 and limma v.3.34.9 for micro-array analysis; BWA version 0.7.16, Picard version 2.9.4, samtools version 1.9, IGV version 2.4.13, MACS2 (version 2.1.1.20160309, bedtools v2.24.0, voom packge (R 3.23, edgeR 3.12.1, limma 3.26.9), deeptools v2.5.7, MEME suite version 4.9.0 and MEME suite version 4.11.3 for ATAC-seq analysis; NIS Elements software (Nikon Instruments) and Slidebook software (Intelligent Imaging Innovations) for imaging data analysis; The Cell Ranger 1.3 Single-Cell software suite (10× Genomics) and t-distributed stochastic neighbour embedding (tSNE) for scRNA-seq analysis.

For manuscripts utilizing custom algorithms or software that are central to the research but not yet described in published literature, software must be made available to editors/reviewers. We strongly encourage code deposition in a community repository (e.g. GitHub). See the Nature Research guidelines for submitting code & software for further information.

Data

Policy information about availability of data

All manuscripts must include a data availability statement. This statement should provide the following information, where applicable:

- Accession codes, unique identifiers, or web links for publicly available datasets
- A list of figures that have associated raw data
- A description of any restrictions on data availability

Microarray, RNA-seq, ATAC-seq and scRNA-seq data have been deposited in the NCBI Gene Expression Omnibus (GEO) database and are accessible through the GEO SuperSeries accession number: GSE126072. All other relevant data are available from the corresponding author upon reasonable request.

Field-specific reporting

Please select the one below that is the best fit for your research. If you are not sure, read the appropriate sections before making your selection.

☒ Life sciences ☐ Behavioural & social sciences ☐ Ecological, evolutionary & environmental sciences

For a reference copy of the document with all sections, see nature.com/documents/nr-reporting-summary-flat.pdf

Life sciences study design

All studies must disclose on these points even when the disclosure is negative.

Sample size	Sample size was selected to maximize the chance of uncovering mean difference which is also statistically significant.
Data exclusions	No data were excluded.
Replication	All the experimental findings were reliably reproduced as validated by at least two independent experiments.
Randomization	In tumour therapy experiments, at day 12 after tumour inoculation, mice bearing similar size of tumours were randomly divided into groups.
Blinding	Blinding was not relevant to these studies.

Reporting for specific materials, systems and methods

We require information from authors about some types of materials, experimental systems and methods used in many studies. Here, indicate whether each material, system or method listed is relevant to your study. If you are not sure if a list item applies to your research, read the appropriate section before selecting a response.

Materials & experimental systems

n/a	Involved in the study
☐	☒ Antibodies
☐	☒ Eukaryotic cell lines
☒	☐ Palaeontology
☐	☒ Animals and other organisms
☒	☐ Human research participants
☒	☐ Clinical data

Methods

n/a	Involved in the study
☒	☐ ChIP-seq
☐	☒ Flow cytometry
☒	☐ MRI-based neuroimaging

Antibodies

Antibodies used

The following antibodies were used for flow cytometry: Active caspase-3 staining was performed using instructions and reagents from the Active Caspase-3 Apoptosis Kit (BD Biosciences). BrdU staining (pulsed for 18 h) was performed using instructions and reagents from the APC BrdU Flow Kit (BD Biosciences). 7-AAD (Sigma) or fixable viability dye (eBioscience) was used for dead-cell exclusion. anti-IFNγ (XMG1.2), anti-TNF (MAb11), anti-IL-2 (JES6-5H4), anti-CD69 (H1.2F3), anti-CD25 (PC61.5), anti-KLRG1 (2F1), anti-ICOS (7E.17G9), anti-LAG3 (C9B7W), anti-PD-1 (J43), anti-CTLA4 (1B8), anti-TOX (TXRX10), anti-TIM3 (RMT3-23) (all from eBioscience); anti-GZMB (QA16A02), anti-CD49a (HMα1), anti-CD44 (IM7), anti-Ki-67 (16A8), anti-CD127 (A7R34) (all from Biolegend); anti-BrdU (3D4), anti-active caspase-3 (C92-605), anti-pH2A.X-S139 (N1-431) (DNA damage biomarker, which measures phosphorylation of the histone variant H2A.X at Ser13946,47), anti-SLAMF6 (13G3) (all from BD Biosciences); anti-BATF (D7C5), anti-TCF-1 (C63D9) (all from Cell Signaling Technology); anti-CD8α (53-6.7) (from SONY); anti-CD62L (MEL-14) (from TONBO Bioscience). 1:100–1:200 dilution.

The following antibodies were used for western blot: anti-MCPIP1 antibody (604421) (R&D), anti-BATF (D7C5) (Cell Signaling Technology), anti-PTPN2 (E-11) (Santa Cruz Biotechnology), anti-SOCS1 (E-9) (Santa Cruz Biotechnology), anti-Hsp90 (MAB3286) (R&D) and anti-β-actin (8H10D10) (Cell Signaling Technology), and HRP conjugated anti-mouse IgG (W4021) (from Promega). 1:1000 – 1:5000 dilutions.

The following antibodies were used for imaging: anti-mCherry (Biorbyt orb11618), anti-GFP (Rockland Immuno 600-401-215), anti-TCF-7 (C63D9) (Cell Signaling Technology 2203), and anti-Tom20 (2F8.1) (Millipore MABT166). 1:100–1:200 dilution.

Validation

The specificities of listed FACS antibodies have been validated by the manufacturer by flow cytometry.
The specificities of listed WB antibodies have been validated by the manufacturer by western blot.
The specificities of listed imaging antibodies have been validated by the manufacturer by imaging.

Eukaryotic cell lines

Policy information about cell lines

Cell line source(s)	B16 F10 and HEK293T cell lines were purchased from ATCC. B16 Ova cell line was kindly provided by Dr. Dario Vignali. huCD19-Ph+ B-ALL cell line was provided by Dr. Terrence Geiger.
Authentication	Cell lines were not authenticated.
Mycoplasma contamination	Cell lines were not tested for mycoplasma contamination.
Commonly misidentified lines (See ICLAC register)	No commonly misidentified cell lines were used.

Animals and other organisms

Policy information about studies involving animals; ARRIVE guidelines recommended for reporting animal research

Laboratory animals	C57BL/6, OT-I, pmel-1 and Rosa26-Cas9 knockin mice were purchased from The Jackson Laboratory. CAR-T transgenic mice were provided by Terrence Geiger (to be described elsewhere). We crossed Rosa26-Cas9 knockin mice with OT-I, pmel-1 or CAR-T transgenic mice to express Cas9 in antigen-specific CD8+ T cells. Gender-matched mice were used at 7–16 weeks old unless otherwise noted.
Wild animals	The study did not involve wild animals.
Field-collected samples	The study did not involve samples collected from the field.
Ethics oversight	Experiments and procedures were performed in accordance with the Institutional Animal Care and Use Committee (IACUC) of St. Jude Children's Research Hospital.

Note that full information on the approval of the study protocol must also be provided in the manuscript.

Flow Cytometry

Plots

Confirm that:

☒ The axis labels state the marker and fluorochrome used (e.g. CD4-FITC).

☒ The axis scales are clearly visible. Include numbers along axes only for bottom left plot of group (a 'group' is an analysis of identical markers).

☒ All plots are contour plots with outliers or pseudocolor plots.

☒ A numerical value for number of cells or percentage (with statistics) is provided.

Methodology

Sample preparation	The spleens and peripheral lymph nodes (PLNs) were gently separated under nylon mesh using the flat end of a 3-mL syringes. Red blood cells were removed by ACK lysing buffer, followed by washing cells with isolation buffer. After spinning down, the cell pellets were resuspended and filtered with nylon mesh before staining. For the examination of tumour infiltrating lymphocytes, tumours were excised, minced and digested with 0.5 mg/ml Collagenase IV (Roche) + 200 UI/ml DNase I (Sigma) for 1 h at 37 °C, and then passed through 70-µm filters to remove undigested tumour tissues. TILs were then isolated by density-gradient centrifugation over Percoll.
Instrument	LSRII or LSR Fortessa (BD Biosciences)
Software	Flowjo 9.9.4 or later (Tree Star)
Cell population abundance	The purities of the sorted sgRNA transduced cells were more than 98%.
Gating strategy	Based on the pattern of FSC-A/SSC-A, cells in the lymphocyte gate were used for analysis of T cell subsets. Singlets were gated according to the pattern of FSC-H vs. FSC-A. Positive populations were determined by the specific antibodies, which were distinct from negative populations.

☒ Tick this box to confirm that a figure exemplifying the gating strategy is provided in the Supplementary Information.